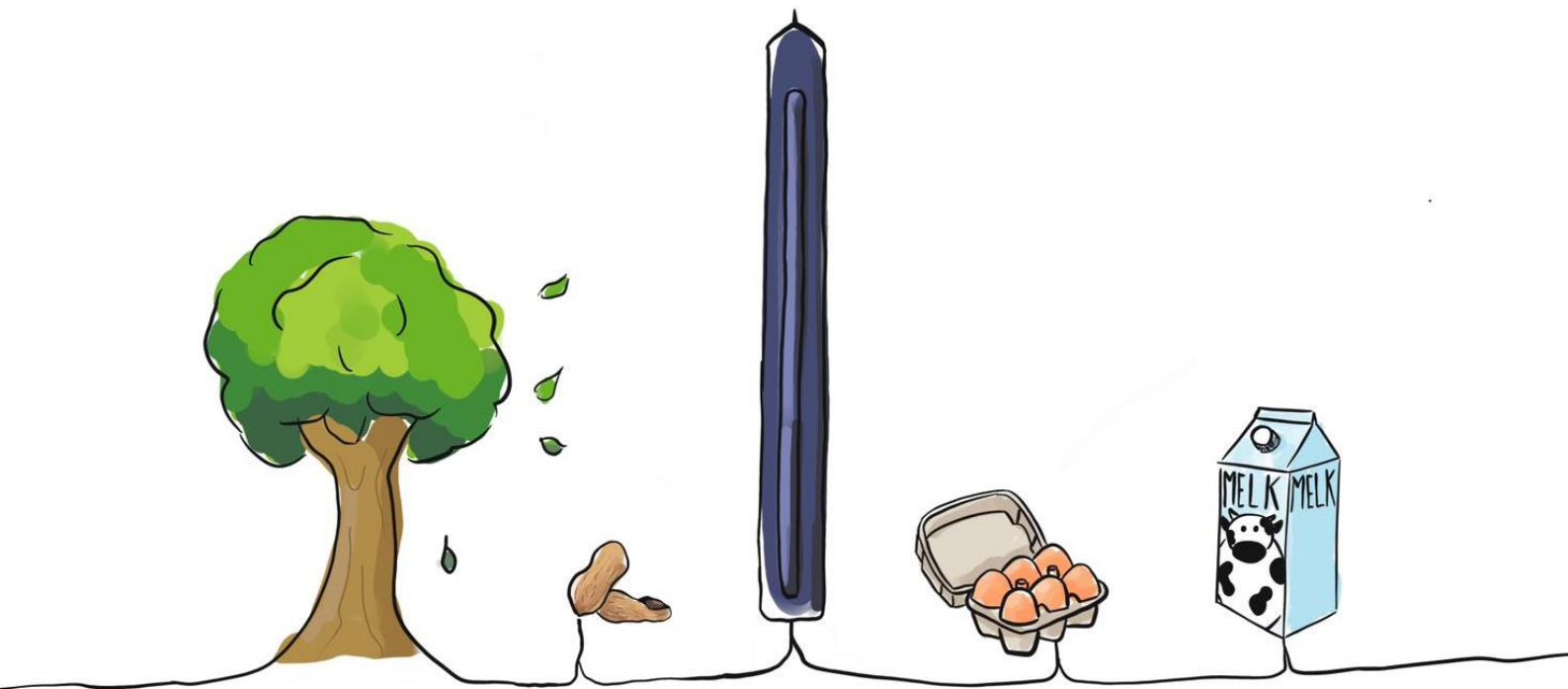


# The effect of the injection depth and injection volume on the wheal size in the Skin Prick Test

- Jamila de Jong -



Thesis for Master of Science  
Technical Medicine | Medical Imaging and Interventions

# The effect of the injection depth and injection volume on the wheal size in the Skin Prick Test

- Jamila de Jong -

6 April 2023

## Graduation Committee

Chairman | University of Twente

Medical supervisor | Deventer Ziekenhuis

Technical supervisor | University of Twente

Technical supervisor | Deventer Ziekenhuis

Process supervisor | University of Twente

External member | University of Twente

Prof. Dr. J.J. Fütterer

Drs. D.M.W. Gorissen

Dr. F.J. Siepel

Dr. R.F.M. van Doremalen

Drs. P.A. van Katwijk

T. Boers MSc

**UNIVERSITY  
OF TWENTE.**

**Deventer  
ziekenhuis**

# Abstract

## Introduction

Allergies affect a significant part of the paediatric population. Allergy diagnosis is based on clinical symptoms and the patient's history, which can subsequently be confirmed by the Skin Prick Test (SPT). Although the SPT is a frequently used diagnostic tool in allergy practices, the results can be affected by a variety of performance factors. Therefore, this study aims to relate the injection depth and injection volume to the wheal size in the SPT to improve the reproducibility and reliability of the test in the future.

## Method

The injection depth was investigated in clinical practice to gain insight into the forces applied on the lancet during the SPT. A soft and hard prick were defined by measuring the force applied on the lancet done by four medical assistants. Thereafter, experiments on *ex vivo* skin were executed to explore the relation between the injection depth and injection volume using OCT and fluorescence. The effect of the injection depth on the wheal size was also investigated by performing the SPT on healthy volunteers. The wheal size induced by a soft and hard prick were statistically compared by a paired samples T-test. At last, direct and indirect injections in agarose gel were compared using the needle-free injector as an alternative for the lancet in the future.

## Results

A soft prick was defined as 5 grams and a hard prick as 60 grams and these values were used during the experiments in this study. The results of the *ex vivo* skin experiments showed contradictory results and a low correlation between the injection depth and volume was found. The study in healthy volunteers showed a significant difference between the mean wheal sizes induced by a soft prick 3.98 mm<sup>2</sup> versus a hard prick 5.82 mm<sup>2</sup> ( $p < 0.001$ ).

## Conclusion

The findings suggest that an increase in injection depth leads to an increase in wheal size. This could result in false negative SPT results, overdiagnosis or medicalisation. Therefore, it is highly recommended to standardise the SPT performance to obtain reproducible and reliable SPT results. Future research must focus on exploring devices to standardise the SPT performance, for example an auto-injector or needle-free injector.

# Table of content

<b>1. General introduction</b>	7
<b>2. The force applied on the lancet in clinical practice</b>	
2.1 Introduction	12
2.2 Method	13
2.2.1 Soft and hard prick definition	14
2.2.2 Movement of the lancet and skin upon injection	14
2.3 Results	14
2.3.1 Soft and hard prick	14
2.3.2 Movement of the lancet and skin upon injection	15
2.4 Discussion	15
2.4.1 Results	15
2.4.2 Limitations	16
2.5 Conclusion	16
<b>3. Phase I: The relation between the injection depth and injection volume in <i>ex vivo</i> skin</b>	
3.1 Introduction	18
3.2 Method	18
3.2.1 Skin preparation	21
3.2.2 Skin Prick Test	21
3.2.3 Skin quality assessment	21
3.2.4 Injection depth determination	21
3.2.5 Injection volume determination	22
3.3 Results	22
3.3.1 Skin quality assessment	22
3.3.2 OCT images	22
3.3.3 Injection depth and volume	23
3.4 Discussion	25
3.4.1 Results	25
3.4.2 Limitations	25
3.4.3 Future recommendations	26
3.5 Conclusion	26
<b>4. Phase II: The relation between the injection depth and wheal size in healthy volunteers</b>	
4.1 Introduction	28
4.2 Method	28
4.2.1 Skin Prick Test	28
4.2.2 Wheal size	29
4.2.3 Statistical analysis	29
4.2.4 Test measurement	29
4.3 Results	29
4.4 Discussion	30
4.4.1 Results	30
4.4.2 Limitations	31
4.5 Conclusion	31
<b>5. Needle-free injection as future perspective in the Skin Prick Test</b>	
5.1 Introduction	33
5.2 Method	33

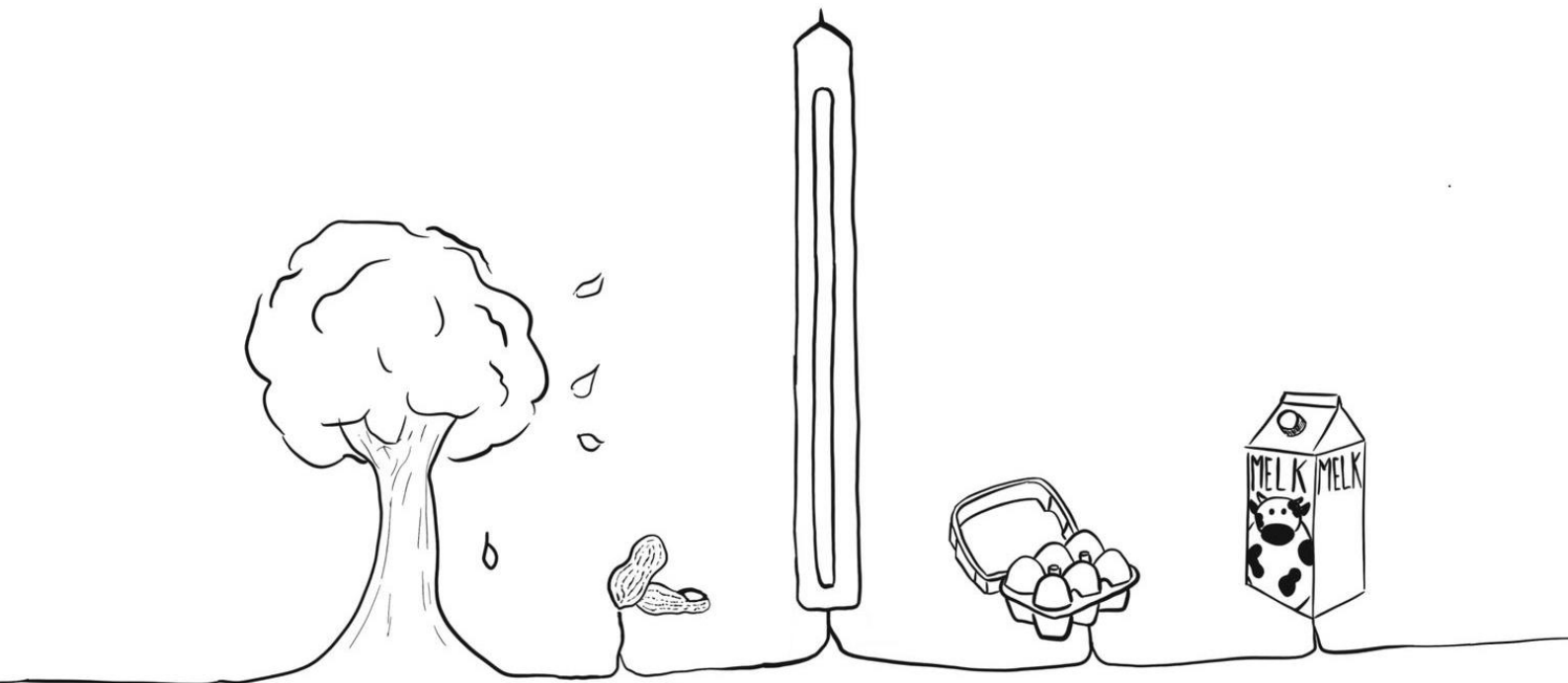
5.2.1 Experiments.....	34
5.2.2 Data acquisition.....	35
5.2.3 Data analysis.....	35
5.3 Results.....	35
5.3.1 Timelapse.....	36
5.3.2 Mean and range.....	36
5.3.3 Visualisation of results.....	36
5.4 Discussion.....	38
5.4.1 Results.....	38
5.4.2 Limitations.....	39
5.5 Conclusion.....	39
<b>6. Impact and future recommendations</b>	
6.1 Clinical impact.....	41
6.2 Future recommendations.....	41
6.3 Conclusion.....	42
<b>7. References</b> .....	44
<b>8. Appendix</b>	
I. MATLAB script – injection depth.....	48
II. Calibration curve.....	49
III. MATLAB script – wheal size.....	50
III.I Wheal surface.....	50
III.II Wheal diameter.....	51
IV. Overview of the segmentation steps.....	52

# List of Abbreviations

APC	antigen-presenting cell
DC	dispersion compensation glass
F	short-pass filter
FcεR1	high-affinity IgE receptor
FDA	Food and Drug Administration
HEWS	Histamine Equivalent Wheal Size
Ig	immunoglobulin
IL	interleukins
L	lens
MA	medical assistants
MHC-II	major histocompatibility complex II
NDF	neutral density filter
OCT	Optical Coherence Tomography
PFV4	Photron FASTCAM Viewer 4
RhoB	rhodamine B
SPT	Skin Prick Test
TCR	T-cell receptor
T <sub>H</sub> 2	T-helper 2
VC	vertical pressure and rotation of 90 degrees clockwise
VCC	vertical pressure and rotation of 90 degrees clockwise and counter-clockwise
VP	vertical pressure
μg	microgram
μL	microlitre
μm	micrometre
μs	microsecond
°	degrees
°C	degrees Celsius
λ	wavelength
a	gravitational acceleration
A	ampere
cm	centimetre
F	Force
fps	frames per second
g	gram
J	joule
m	mass
m	meter
mm <sup>2</sup>	square millimetre
mg	milligram
mL	millilitre
mm	millimetre
ms	millisecond
N	Newton
nm	nanometre
P	power
s	second
U	units
V	voltage
W	wattage
wt.	weight

# Chapter 1

## General introduction



Allergies affect a significant part of the paediatric population; 5% of the Dutch children develop an allergy and the prevalence in westernised countries has only been rising in recent decades.<sup>1,2</sup> The most common allergies in children can be divided into two categories: inhalant and food allergies. These allergies are classified as Type I Hypersensitivities and are characterised by an immune response to an allergen and the release of immunoglobulin E (IgE).<sup>3</sup> The immune response to an allergen consists of two phases: in the sensitisation phase there is the initial contact of the allergen with the immune system and the elicitation phase is the subsequent exposure which can result in an allergic reaction.<sup>4</sup> During the sensitisation phase, the allergen is bound to the major histocompatibility complex II of the antigen-presenting cell and presented to the T-helper 2 (T<sub>H</sub>2) cell. The T<sub>H</sub>2 secretes interleukins IL-4, IL-5 and IL-13 that activate B-cells to differentiate into IgE-producing plasma cells.<sup>3,5</sup> The produced IgE binds on the high-affinity IgE receptor (FcεR1) on mast cells and basophils in connective tissue and mucosa.<sup>6</sup> If a subsequent exposure occurs, the allergen cross-links with the IgE-FcεR1 complex resulting in mast cell or basophil degranulation and the release of chemical mediators, such as histamine, leukotrienes, prostaglandins and cytokines.<sup>3,5-7</sup> This process is illustrated in Figure 1.

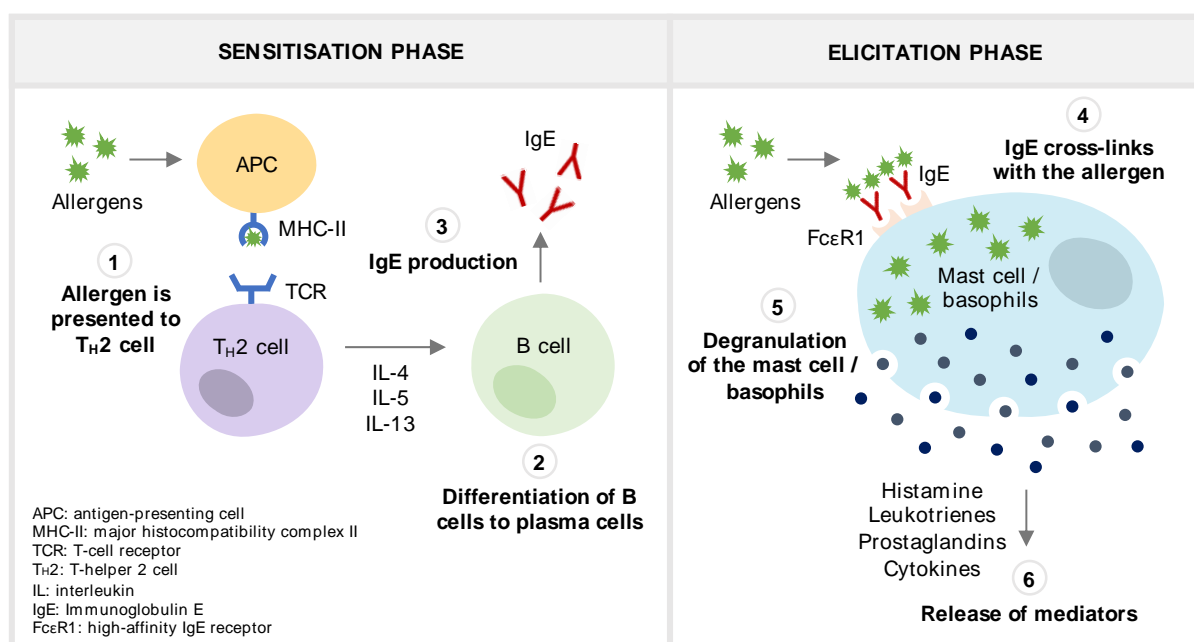


Figure 1: The left image shows the sensitisation phase, the initial contact of the allergen with the immune system and the right image shows the elicitation phase, subsequent exposure which can result in an allergic reaction.

The immune response can lead to clinical symptoms, for example, inhalant allergies can cause sneezing, rhinorrhoea, nasal obstruction, conjunctivitis and pruritis. In addition, the persistence of these symptoms can affect school performance, sleep quality, productivity, concentration and social life.<sup>8</sup> Food allergies can manifest as angioedema, urticaria, abdominal pain, pulmonary reactions or anaphylaxis.<sup>3</sup> The diagnosis of an inhalant or food allergy is based on these clinical symptoms and the patient's and family history. It is important to obtain a full history including frequency, duration and timing of reactions, symptoms, previous exposure and triggers to determine if the patient experienced an allergic reaction.<sup>3,8</sup> Allergy diagnosis can be confirmed by IgE sensitisation tests.

The first test that can provide evidence for sensitisation to an allergen is the serological test which detects circulating IgE antibodies in the blood against a specific antigen. The test can be performed for a single antigen or four multiple antigens.<sup>9</sup> The result of the test is negative when the concentration of the IgE specific antigens is < 0.35 U/mL. This means that the patient is not sensitised or has never been in contact with the allergen. A value > 0.35 U/mL increases the risk of an allergy but does not confirm the diagnosis because sensitisation does not always have clinical consequences.<sup>10</sup> The second test that can be performed to test sensitisation is the SPT.

The skin test was invented in 1880 by Charles H. Blackley, a physician suffering from hay fever. He experimented on this forearm where he abraded a small area with a lancet. He applied grass pollen and a strip of adhesive plaster to the damaged area and after a few minutes a wheal appeared, the first scratch test was executed.<sup>11</sup> Thomas Lewis argued in 1924 that a fine needle led to similar results and the scratch test was replaced by the SPT.<sup>12</sup> The first article about the SPT was published in 1959 by Helmtraud Ebruster who investigated the test extensively and his protocol is applied in clinics up to this date.<sup>7</sup>

The SPT is performed on the skin surface of the flexor aspect of the forearm or the back. The skin is composed of three layers: epidermis, dermis and hypodermis. The epidermis is a keratinised epithelium and can be divided into five layers: Stratum Corneum, Stratum Lucidum, Stratum Granulosum, Stratum Spinosum and Stratum Basale.<sup>13,14</sup> The Stratum Spinosum is densely populated with Langerhans cells which are antigen-presenting cells and play an important role in the skin reaction during the SPT.<sup>15,16</sup> Droplets of allergen extracts and a positive (histamine) and negative (saline) control are pricked into the epidermis with a small lancet. A new lancet is used for each allergen to prevent contamination. The allergen is absorbed into the epidermis and if a child is sensitised the Langerhans cells induce an immune response and a wheal, an itchy bump surrounded by erythema, appears on the skin.<sup>17</sup> The positive control must induce a wheal  $\geq 3$  mm in diameter and the negative control should not affect the skin for the test to be considered reliable. After 15 minutes, the size of the emerging wheals is measured by outlining the contours with a pencil. Adhesive tape is used to transfer the markings to paper and the mean diameter is measured and the Histamine Equivalent Wheal Size (HEWS) is calculated. The mean diameter of the wheal is the average of the longest orthogonal diameters. The HEWS is the ratio between the mean diameter of the allergen and the histamine wheal.<sup>18</sup> The steps of the SPT are illustrated in Figure 2.

The result of the SPT is negative when the applied allergen does not induce a wheal on the skin. This means that sensitisation to the tested allergen is absent. In case the result of a food allergen is negative, the recommendation is to introduce the food product at home. The cut-off value for a positive SPT is a HEWS  $\geq 0.4$  mm for inhalant and food allergies or a wheal diameter  $> 3$  mm.<sup>18</sup> When an inhalant allergen induces a positive outcome, the clinical symptoms are evaluated and medication can be started to reduce the symptoms. A positive SPT to a food allergen enhances the risk of an allergy and this can be confirmed by an oral food challenge. During the oral food challenge, the suspected allergen is administrated orally in increasing doses to identify the tolerability, threshold and symptom severity.<sup>19</sup>

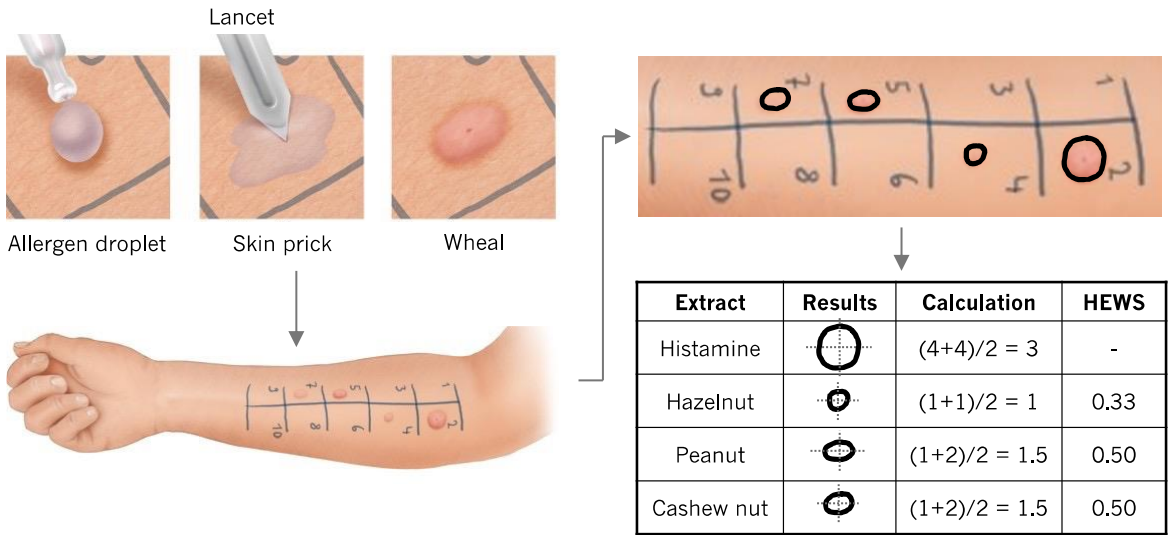


Figure 2: The different steps of the SPT. First the allergen droplets are pricked into the skin. If a child is sensitised a wheal, an itchy bump surrounded by erythema, appears on the skin. The size of the emerging wheals is measured by outlining the contours with a pencil. Adhesive tape is used to transfer the markings to paper and the mean diameter is measured and the HEWS is calculated.

The Deventer Hospital is currently focussing on automatic reading of the SPT results to improve the patient outcome prediction. However, several studies reported that the results are not only influenced by the SPT reading but are also affected by a variety of performance factors.<sup>20-22</sup> The first factor that can affect the SPT performance is the commercial availability of different SPT puncturing devices (section 2.1) which are applied in clinical practice around the world. Many studies compared different SPT devices, and a great variability has been reported regarding sensitivity, specificity, inter- and intra-observer agreement, and pain score.<sup>21,22,31,23-30</sup> This could be explained by the fact that each device has a unique puncture tip and interrupts the skin to a different extent. The trauma imparted to the skin does also depend on the amount of pressure applied on the device, the angle of application and lancet weight resulting in a variability of injection depths.<sup>20,32</sup> Østerballe and Weeke *et al.* argued that the wheal size increased until the prick depth reached 1 mm, assuming that the injection depth equals the size of the lancet tip but further research is lacking.<sup>33</sup> In previous SPT studies, the injection depth was described as applying moderate pressure on the lancet which was estimated to correspond to a skin depression of about 2 to 3 mm.<sup>25,27</sup> Other researchers described the pricking as applying (light) vertical or direct pressure on the lancet, but exact injection depth measurements are missing.<sup>34</sup> Moreover, the injection volume of the positive control, negative control and allergen extracts is an unexplored field of study, and to date it is unknown how much liquid is injected during the test. Previous studies have reported injection volume estimations of 0.01-0.05 mL, but evidence is missing.<sup>35-39</sup> If the before mentioned parameters lead to unreliable SPT results, this could lead to medicalisation and unnecessary oral food challenges, but also to untreated inhalant allergies or unsafe home introductions of food products. Therefore, it is important to not only investigate the SPT reading but also explore the effect of the SPT performance on the test outcomes.

This proof-of-concept study aims to relate the injection depth and injection volume to the wheal size to improve the reproducibility and reliability of the SPT in the future. This leads to the following research question:

*How are the injection depth and injection volume related to the wheal size in the Skin Prick Test using a lancet?*

The hypothesis is that an increase in injection depth results in an increase in injection volume and an increase in wheal size. The study consists of two phases: relating the injection depth to the injection volume on *ex vivo* skin (phase I) and relating the injection depth to the wheal size in healthy volunteers (phase II). This leads to the following subquestions:

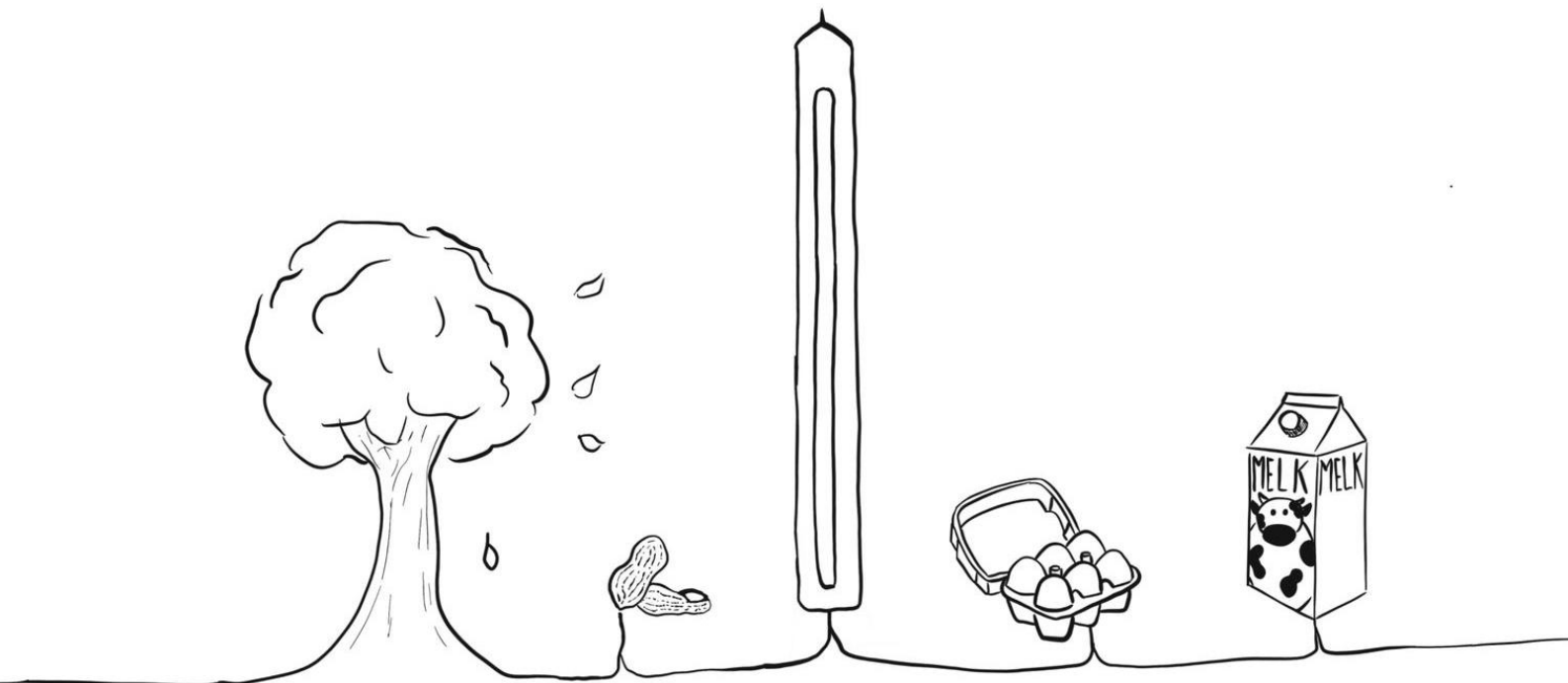
1. *How is the injection depth related to the injection volume using the lancet in porcine skin and ex vivo human skin?*
2. *How is the injection depth related to the wheal size using the lancet in healthy volunteers?*

The injection depth, injection volume and wheal size will be determined as follows. The injection depth is measured using Optical Coherence Tomography (OCT). This imaging technique is a biomedical, non-contact, optimal imaging technique that can visualise the internal structures in biological tissues. OCT can image *in vivo* tissues in real time by measuring backscattered light with an axial resolution of 1 to 15  $\mu\text{m}$  and a maximum depth of 2 to 3 mm.<sup>40</sup> The injection volume is quantified by the intensity of the emission spectra of fluorophore labelled histamine pricked into the *ex vivo* skin. Fluorescence is the emission of light after a molecule or atom absorbs light or radiation.<sup>41,42</sup> The injection volume is determined as mass but the term volume will be used in this thesis to make clear that it refers to the amount of injected substance. The wheal size is calculated by photographing the forearm and manually select and segment each wheal.

The research question and subquestions will be answered in this thesis. The first chapter provides an insight into the force applied on the lancet in clinical practice to define a soft and hard prick. The second chapter describes the experiments performed on *ex vivo* porcine and human skin to investigate the relation between the injection depth and injection volume. The next chapter discusses the study in healthy volunteers to relate the injection depth to the wheal size. A pilot study of the needle-free injector as a future perspective is written in Chapter 5. The last chapter describes the impact and future recommendations.

# Chapter 2

The force applied on the lancet  
in clinical practice



## 2.1 Introduction

The SPT is performed around the world and different devices are used to prick the allergens into the skin. The devices can be divided into single-headed and multi-headed devices. Single-headed devices comprise one tip to prick one droplet at a time into the epidermis. The most commonly used prick devices consist of one spike such as the Oryum (Yilmaz Medikal, Gaziantep, Turkey), QUINTIP (HollisterStier, Spokane, Washington), ALK (ALK, Hørsholm, Denmark), Stallerpoint and Stallergenes (Stallergenes, Antony, France). The lancet can be manufactured from metallic, plastic or a combination of materials. The case and tip can have different shapes and characteristics to optimize the injection quality and reduce pain. For instance, the lancet can have a long triangular shape (ALK and Stallergenes) or a steel needle shape with surrounding plastic guards to limit the injection depth (Oryum, QUINTIP and Stallerpoint). The tip of the lancet can also contain multiple spikes. For example, the Duotip-Test II (Lincoln Diagnostics, Decatur, Illinois) tip is split into two sharp points and the GREER Pick (Greer, Lenoir, North Carolina) tip consists of seven spikes. The ALK lancet is used in Deventer Hospital.

Two studies compared different application techniques of single-headed devices: vertical pressure (VP), vertical pressure and rotation of 90° clockwise (VC) and vertical pressure and rotation of 90° clockwise and counter-clockwise (VCC). Kahveci *et al.* used the Oryum lancet and found an increase in wheal size and a higher false-positivity rate after VC and VCC compared to VP.<sup>23</sup> The second study reported similar results using the Stallerpoint lancet; an increase in wheal size and flare after VC and VCC.<sup>22</sup> In addition, pain score was included and children stated a Wong-Baker FACES Pain Rating Scale of 2 after VP and VC, and 4 after VCC. These studies showed that the applied technique can affect the wheal size and perception of the test and that applying VP leads to fewer false-positive results and a low pain score.

Multi-headed devices consist of connected single-headed devices to prick up to ten allergens simultaneously into the skin by dipping the device first in the extract bottles.<sup>43</sup> The advantages of multi-headed devices are time efficiency, greater acceptability of patients and the fixed insertion angle.<sup>20,21</sup> On the contrary, studies have shown that the inner lancets produce statistically smaller wheals compared to the outer lancets of the multi-headed devices.<sup>44</sup> Several multi-headed devices are FDA approved: Multi-Test II and Multi-Test PC (Lincoln Diagnostics, Decatur, Illinois), ComfortTen (HollisterStier, Spokane, Washington), Quick-Test (Panatrex, Placentia, California), Quintest (Bayer Allergen Products, Spokane, Washington), GREER Track and OMNI (Greer, Lenoir, North Carolina). Comparable to single-headed devices, multi-headed devices can consist of different tips. For example, the Multi-Test II tip has similar characteristics as the GREER Pick and ComfortTen tip is comparable to QUINTIP. Multi-headed devices are not applied in the Netherlands. Figure 3 presents an overview of single- and multi-headed devices.

In Deventer Hospital, medical assistants use the ALK lancet to prick the allergens with VP into the skin according to the SPT protocol and the assistants aim to prick the allergens with a constant force. However, the force on the lancet is difficult to repeat and the force concerning immunological response and patient comfort is unexplored.<sup>45</sup> Therefore, it is important to gain insight into the range of forces applied on the lancet in daily practice. This results can be used to relate the injection depth to the injection volume and wheal size in this study. To inspect the force, two experiments were performed: 1) the applied force on the lancet was measured during injection to determine the minimum (soft prick) and maximum (hard prick) injection depth and 2) the movement of the lancet and skin upon injection was visualised. Based on the results of these experiments, the soft and hard pricks were defined for the follow-up experiments on ex-vivo skin (Chapter 3) and the study in healthy volunteers (Chapter 4).



Figure 3: Overview of single- and multi-headed devices.

## 2.2 Method

The first experiment in this study aimed to measure the applied force on the lancet by using a skin phantom and a balance. The skin phantom was composed of different structures to mimic the layers of the skin but differed in haptic feedback compared to human skin. Clinicians rely on haptic feedback in performing needle insertion procedures and it is therefore a crucial factor in obtaining reliable results in this experiment.<sup>46,47</sup> Therefore, the medical assistants pricked alternately in the skin phantom and a forearm to take the haptic feedback into account.

The balance was used to measure the force on the lancet during injection. The weights are related to the applied forces by the following equation:

$$F = m * a \quad (1)$$

Where  $F$  is force in Newton,  $m$  is mass in grams and  $a$  is gravitational acceleration in  $m/s^2$ . The gravitational acceleration on earth is  $9.81 m/s^2$ .

The second experiment visualised the movement of the lancet and skin upon injection. The interaction between the upper skin layers and the lancet in the SPT is not described in literature to date but one previous study described the effect of the skin characteristics on the penetration of microneedles.<sup>48</sup> They reported that the skin showed a displacement of  $\sim 450 \mu m$  applying a force of  $0.35 N$  before the microneedle penetrated the epidermis. The amount of force and displacement depended on the skin stiffness during puncture which was determined by the conditions of the stratum corneum. The presence of collagen and elastin in the dermis was also an important component which contributed to the mechanical

response. The expectation was that the skin reacted similar to the lancet in this experiment and would first show a displacement before the lancet penetrated the epidermis.

## 2.2.1 Soft and hard prick definition

The experiments were performed at Deventer Hospital. A skin phantom (MediStitch, Duiven, the Netherlands) was placed on a precision scale (BrandNewCake, Goor, the Netherlands) to measure the force during injection. The precision scale had a resolution of 0.01 g and a maximum load of 200 g.

Four experienced medical assistants pricked ten times into the skin phantom using the ALK lancet. They pricked alternately in the skin phantom and the volar aspect of the researcher's forearm to increase the reliability of the measurements. The experiments were recorded in slow-motion with an iPhone (SE 2020, Apple) to read out the peak weights on the precision scale of each injection. The data was analysed in Excel (2022) and the minimum and maximum values of all the peak weights were calculated.

The minimum and maximum value of the peak weights were set to a Force Gauge, an instrument to quantify the applied force. The Force Gauge-lancet setups are illustrated in Figure 4 and were used to control the soft and hard prick during the follow-up experiments on *ex-vivo* skin and the study in healthy volunteers.

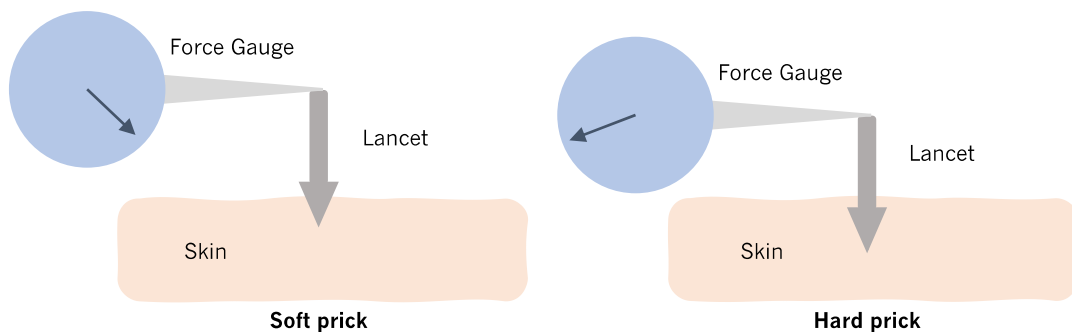


Figure 4: Illustration of a soft and hard prick using the Force Gauge-lancet setup. The Force Gauge for the soft prick is ranged from 0 to 15 g and for the hard prick from 0 to 250 g.

## 2.2.2 Movement of the lancet and skin upon injection

The experiments were performed at the Mesoscale Chemical Systems research department of the University of Twente. Two injections were performed on the forefinger: 1) the ALK lancet was pricked directly into the skin and 2) the ALK lancet was pricked through a water droplet into the skin to simulate the SPT. The Force Gauge was not fixed to the lancet during these experiments. Both injections were executed eight times by the researcher and recorded using a high-speed camera (Photron Fastcam SA-X2 1080K-M2). The images were captured at 200 frames/second (fps) with additional illumination from a LED light source (SCHOTT). The camera was triggered by the movement of the lancet into the field of view. The resolution of the images was 512 x 1024. The injections were analysed in Photron FASTCAM Viewer 4 (PFV4) and the recordings with the highest quality regarding sharpness, contrast and brightness were analysed.

## 2.3 Results

### 2.3.1 Soft and hard prick

In total, 40 pricks were executed by four medical assistants. Two pricks performed by the fourth medical assistant were excluded because the precision scale could not measure the peak weight of the injection due to the injection speed. The results are shown in Table 1. The minimum and maximum value of all measured peak weights were respectively 0.03 and 58.06 g.

Table 1: Weights of the experiments subdivided by the four medical assistants (MA).

	MA 1 (g)	MA 2 (g)	MA 3 (g)	MA 4 (g)
1	28.98	3.27	0.03	34.41
2	41.68	0.67	4.50	7.44
3	58.06	0.22	0.47	11.19
4	18.09	0.10	2.91	3.79
5	23.36	3.87	4.24	4.88
6	27.46	2.90	0.70	-
7	14.84	0.13	2.13	12.39
8	15.77	0.84	0.45	1.73
9	19.45	1.82	4.45	1.77
10	20.11	3.71	1.01	-
<b>Minimum</b>	14.84	0.10	0.03	1.73
<b>Maximum</b>	58.06	3.87	4.50	34.41

The 6<sup>th</sup> and 10<sup>th</sup> prick are the missing values of the fourth medical assistant.

### 2.3.2 Movement of the lancet and skin upon injection

The timelapses of the injection directly into the skin and the injection through a water droplet into the skin are shown in Figure 5. The lancet of the direct injection entered the skin at  $t = 30 \mu\text{s}$  and reached the deepest injection point at  $t = 320 \mu\text{s}$ . The lancet was pulled back from the skin and lifted the upper layers of the epidermis before skin contact was broken ( $t = 540 \mu\text{s}$ ). The lancet of the indirect injection contacted the droplet at  $t = 0 \mu\text{s}$ . Van der Waals forces and hydrogen bonds increased the surface tension and the droplet adhered to the tip of the lancet ( $t = 15 \mu\text{s}$ ). The lancet entered the skin at  $t = 180 \mu\text{s}$  and the deepest injection point was reached at  $t = 230 \mu\text{s}$ . The water droplet adhered to the lancet tip when the lancet moved out of the skin ( $t = 380 \mu\text{s}$ ) and the contact was broken at  $t = 400 \mu\text{s}$ .

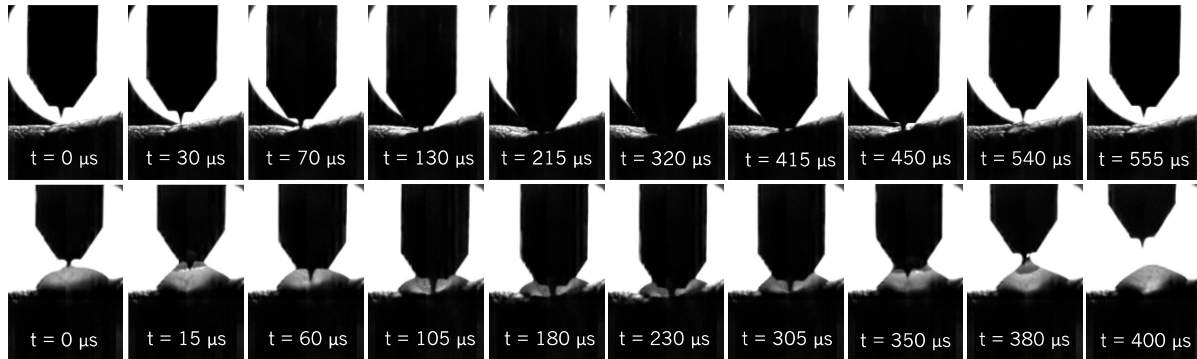


Figure 5: Timelapse of the injection directly into the skin and the injection through a water droplet into the skin recorded with the high-speed camera. The shutter speed of the camera was  $1/4000000$  s. The field of view was  $512 \times 1024$  pixels.

## 2.4 Discussion

### 2.4.1 Results

The experiments aimed to gain insight into the range of injection depths in daily clinical practice to determine the minimum (soft prick) and maximum (hard prick) injection depth for follow-up experiments in this study. The results showed that the minimum weight applied on the lancet was 0.03 g. However, this value is not measurable with the Force Gauge. Therefore, a soft prick is defined as 5 g, the minimum detectable value of the Force Gauge. The maximum weight on the lancet was 58.06 g and this value is rounded up to 60 g to describe a hard prick. The values of a soft and hard prick will be used in the follow-up experiments on *ex-vivo* skin and the study in healthy volunteers. Consistent with literature, the results

show a high intra- and inter-operator variability.<sup>49-51</sup> A finding that stands out is the mean weight applied by medical assistant 1; the mean value (26.78 g) is much higher compared to the other medical assistants. In clinical practice, the SPT is performed by multiple medical assistants which could therefore lead to a variation in applied weights on the lancet. This adds to the growing body of research that emphasizes the importance of standardising the SPT performance.

The movement of the lancet and skin upon injection was visualised to gain more insight into the stages of pricking and the interaction between the skin and the lancet. The timelapse of the direct injection showed that the skin moved with the lancet before penetration which created a bulge in the skin. This bulge blocked the injection spot and complicated the measurement of the lancet tip that penetrated the skin. In both the direct and indirect injections was seen that the horizontal shoulders of the lancet did not touch the skin. This finding differs from that of Østerballe and Weeke *et al.* who argued that the injection depth is standardised by the horizontal shoulders of the lancet, assuming that the complete tip is always injected.<sup>33</sup> When the horizontal shoulders do not touch the skin, the lancet tip is not entirely injected and the pricking depth is not stable. This can cause a great variability of injection depths in clinical practice.

## 2.4.2 Limitations

The experiment has some limitations. First, the applied force was measured using a skin phantom that differs in tactual feedback compared to *in vivo* skin which could influence the results. However, the medical assistants pricked alternately the skin phantom and forearm of the researcher to calibrate the measurements. Furthermore, a computer connected balance could increase the accuracy of the weight measurements. The increase and decrease in weight during a prick could be tracked and transported to the computer to plot the applied weight over time. This could provide more information about the injection compared to measuring the peak weight only. A computer connected balance was not available in this research but is advised for future studies.

The experimental setup of the visualisation could be improved by the addition of light sources. This could lead to less shadow on the skin and an increase in brightness of the images. Moreover, the experiment could be repeated with other SPT devices, application techniques and allergen droplets to visualise and compare different aspects of the SPT.

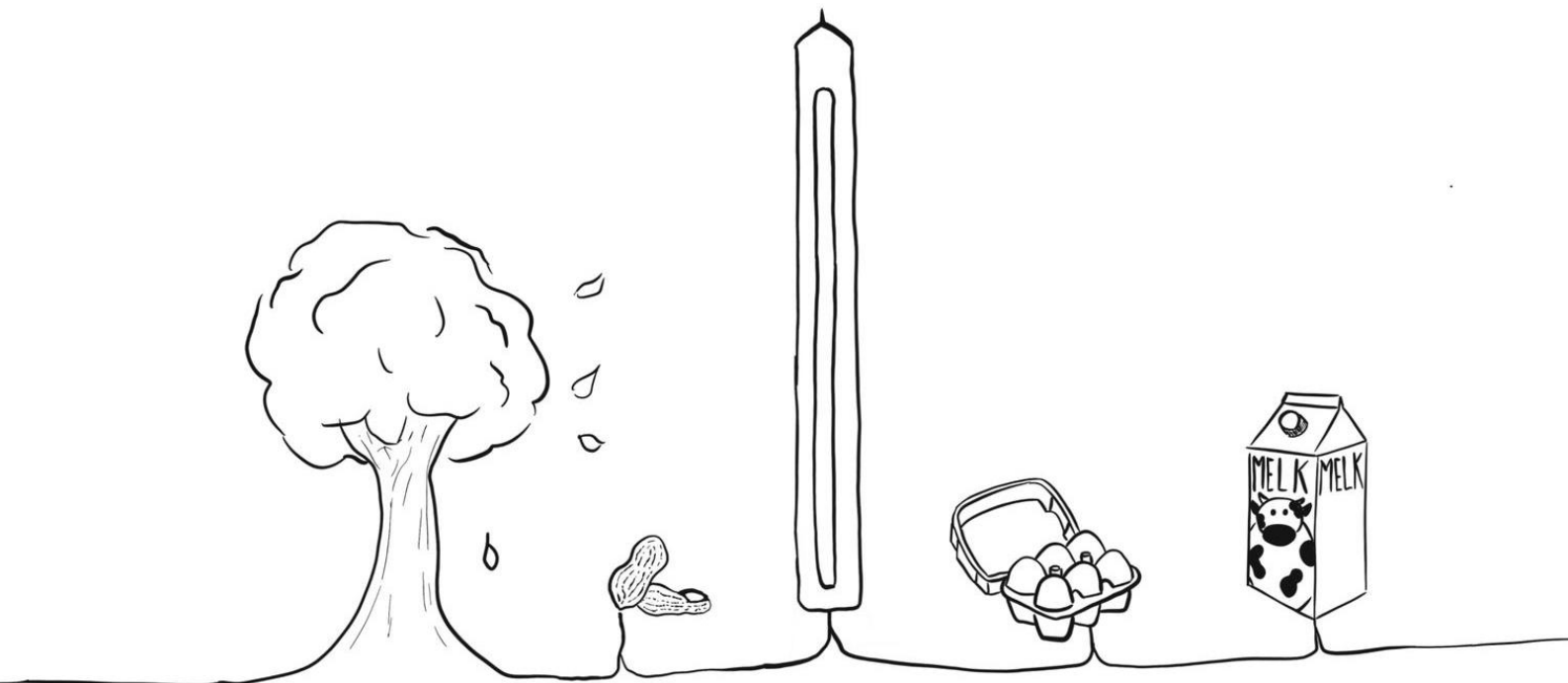
## 2.5 Conclusion

The applied force on the lancet was measured in an SPT simulation setting to estimate the minimum and maximum applied weight in daily clinical practice. These values will be used in the Force Gauge-lancet set-ups to standardise the injection depth in the follow-up experiments on *ex-vivo* skin and the study in healthy volunteers. A soft prick is defined as 5 g and a hard prick as 60 g. The visualisation of the movement of the lancet and skin upon injection showed the formation of a skin bulge the moment before penetration and that the horizontal shoulders of the lancet did not stabilise the injection depth. Further research should focus on measuring the applied force over time and repeating the visualisation with other SPT devices, application techniques and allergen droplets.

# Chapter 3

## *Phase I:*

The relation between the injection depth and injection volume in *ex vivo* skin



## 3.1 Introduction

During the SPT the medical assistants aim to prick the lancet into the skin with constant force, but the results in the previous chapter show that the intra- and inter-operator variability is high. This could lead to a variation in injection depth and volumes within and between patients. To this date, the relation between the injection depth and injection volume is an unexplored field in SPT studies because most researchers have only focussed on the effect of different SPT devices and application techniques on the wheal size. In previous studies, the injection depth was described as applying moderate pressure on the lancet which was estimated to correspond to a skin depression of about 2 to 3 mm.<sup>25,27</sup> Other researchers described the pricking as applying (light) vertical or direct pressure on the lancet, but exact injection depth measurements are missing.<sup>34</sup> Studies argued that the injection depth is standardised by the horizontal shoulders of the lancet tip.<sup>20</sup> The main weakness of this theory is that the entire tip is not always injected in clinical practice (Chapter 2) which results in a variation in injection depth. Therefore, this study aims to explore the relation between the injection depth and the injection volume on *ex vivo* skin. The hypothesis states that an increase in injection depth results in an increase in injection volume because a larger interruption of the skin will lead to a larger capacity that can be filled by the allergen extract.

## 3.2 Method

In this study, the injection depth and injection volume were measured. Histological samples of the porcine and human skin were analysed to assess the quality of the skin. For the injection depth measurements, it was important to find a technology with the following characteristics: 1) fast imaging of the pricking hole after the allergen was pricked into the skin, 2) high resolution because the lancet penetrated the skin only with the lancet tip which has a size of 0.8 mm, and 3) imaging in three directions to select the pricking spot (XY) and measure the injection depth (XZ and YZ). A technique that complies with these conditions and is used in previous studies to measure the injection depth in the epidermis is Optical Coherence Tomography (OCT).<sup>48</sup>

OCT is a biomedical, non-contact, optical imaging technique that can visualise the internal structures in biological tissues. OCT can image *in vivo* tissues in real time by measuring backscattered light with a resolution of 1 to 15  $\mu\text{m}$  and a penetration depth of 2 to 3 mm. This modality has characteristics of both ultrasound and microscopy. Ultrasound has a relatively low resolution but a high penetration depth compared to OCT. Microscopy can only image at a limited depth of a few hundred microns but has a very high resolution. As can be seen in Figure 6, OCT can image tissues at depths and resolutions between ultrasound and microscopy and fills the gap between these two imaging techniques.<sup>52</sup> The technology is based on low coherence interferometry which measures the magnitude and time delay of backscattered light. A Michelson interferometer is the main component of this principle and consists of a light source, beam splitter, reference mirror and detector. The light source emits light to the beam splitter which splits the light into two directions. One light beam travels to the reference mirror at a known distance and is reflected back to the beam splitter. The other light beam travels to the sample and the dispersed light propagates back to the beam splitter. The two combined light beams interfere and travel to the detector.<sup>52</sup> This process is illustrated in Figure 7.

The OCT system used during this study is custom-built at the University of Twente. The light source (SuperK EXTREME EXB-6, NKT Photonics) contains visible light which propagates first through two density filters (ND05A, Thorlabs) to decrease the light intensity. The light is expanded and collimated by three lenses (L1: LD2746-A, L2: LD2060-A, L3: LB1471-A, Thorlabs) and filtered by a short-pass filter (FESH0700, Thorlabs) to remove light with a wavelength  $> 700$  nm. The light enters the Michelson interferometer as described in the previous section. The beam splitter (BS028, Thorlabs) sends 90% of the light to the reference mirror

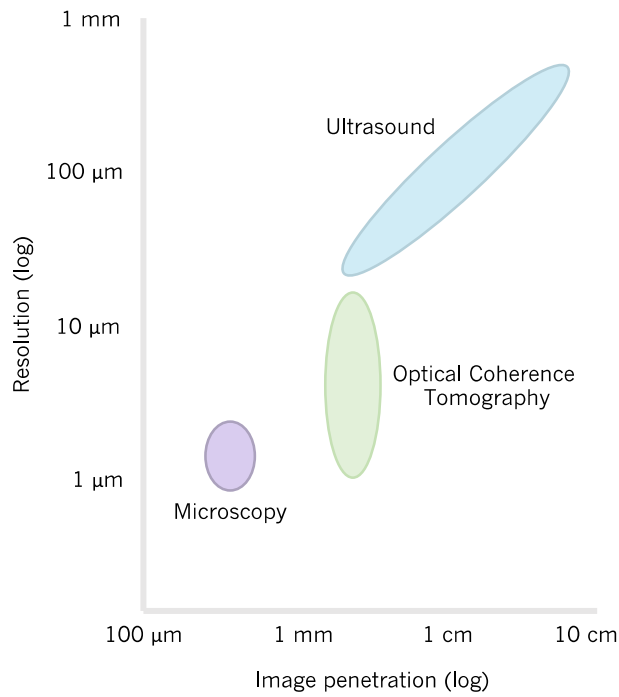


Figure 6: Visualisation of the comparison of microscopy, OCT and ultrasound considering resolution and image penetration.

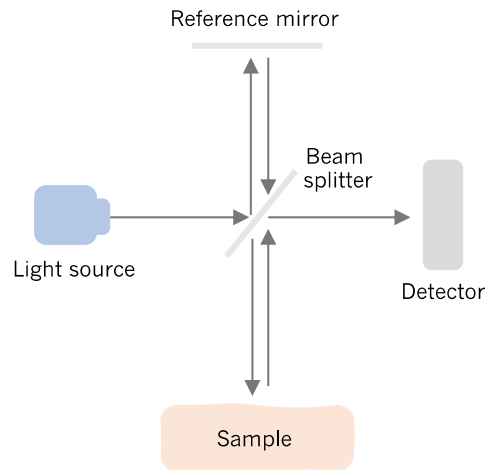
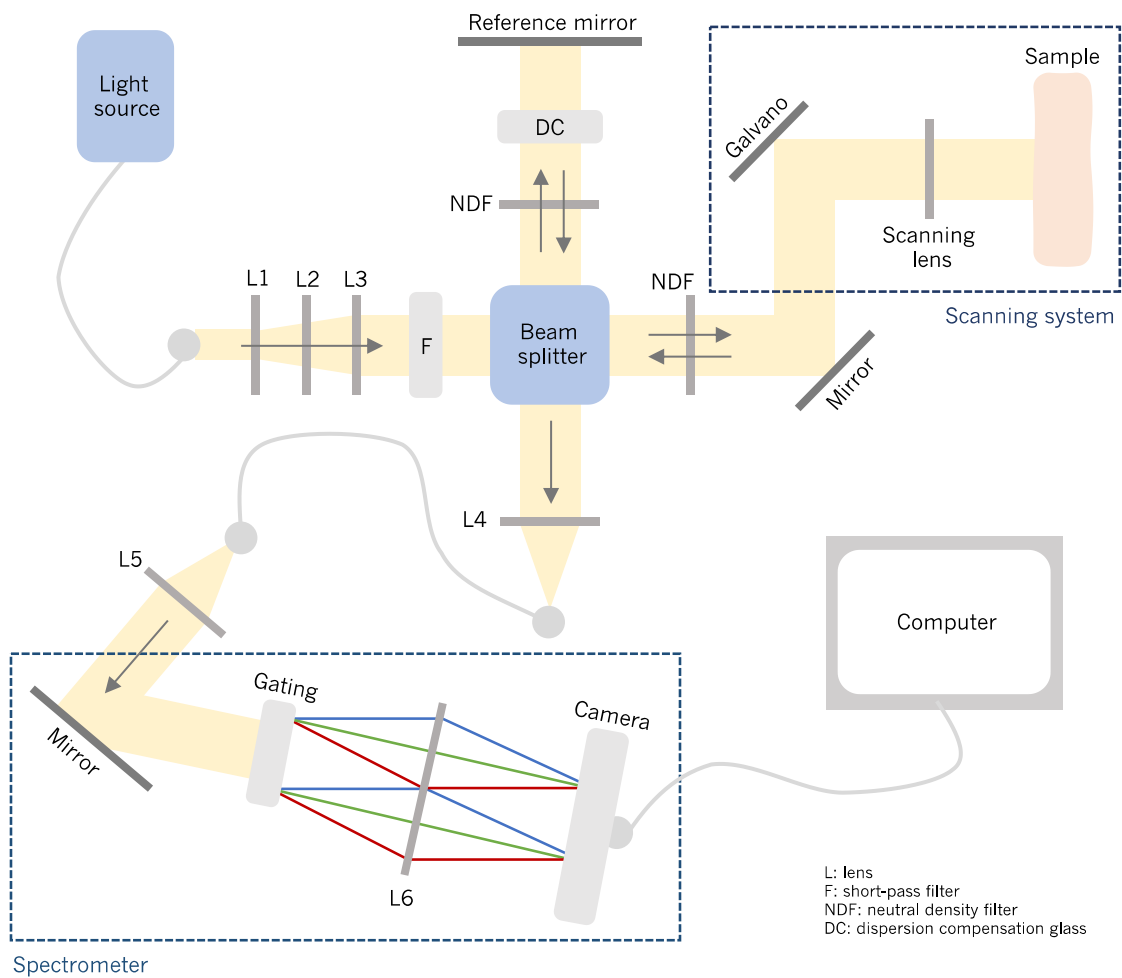


Figure 7: Michelson interferometer.



Spectrometer

Figure 8: Illustration of the OCT system.

and 10% to the sample. A density filter (NDC-50C-4M, Thorlabs) and a dispersion compensation glass (LSM03DC-VIS, Thorlabs) are placed in the reference arm to control the intensity of the light beam and to compensate for the dispersed light from the scanning lens. The reference mirror (PF10-03-P01, Thorlabs) reflects the light back to the beam splitter. Another density filter (NDC-50C-2M-A, Thorlabs) is placed in the sample arm before the light propagates through the galvanometer scanner (8320K, Cambridge Technology). The galvanometer controls the direction of the beam. After adjusting the direction, a scanning lens (LSM03-VIS, Thorlabs) focuses the beam toward the sample. The reflected light from the sample and from the reference mirror are combined at the beam splitter. The combined light is converged and travels through a single-mode fibre (S405XP, Thorlabs) to the spectrometer (HoloSpec f/1.8i, Kaiser Optical Systems). The spectrometer, with a spectral resolution of 0.1 nm in the range of 450 to 650 nm, disperses the light on a line camera (Sprint sPL4096-140km, Basler) to detect the light intensity as a function of the wavelength. To visualise the sample, the intensity values are converted to in-depth information by a fast Fourier transform and displayed using a greyscale. The resolution of this system is 1.3  $\mu\text{m}$ . The complete OCT system is presented in Figure 8.

After the injection depth was determined, the injection volume was measured. A technology that measured the injection volume must be able to detect volumes in the size of micrograms with a high accuracy. A technology that complies with these conditions and was available for this study was fluorescence. Fluorescence is a useful technique in the field of molecular life science to track or visualise biological molecules and processes.<sup>53</sup> Fluorescence is the emission of light after a molecule or atom absorbs light or radiation. First, the fluorescent molecule absorbs photons and the electrons shift from the ground state level to the excited state. Next, vibrational relaxation occurs, the electron shifts to the lowest vibrational state of the first excited state which is a non-radiative process. Thereafter, the electron shifts back to the ground state emitting fluorescence light. This process is illustrated in Figure 9. A small part of the absorbed photons is converted into heat and movement, therefore the emitted photons are lower in energy and have a higher wavelength compared to the absorbed photons.<sup>41,42</sup>

An example of a fluorescent molecule is rhodamine B. The measured fluorescence intensity of rhodamine B is linearly correlated to the number of fluorescent molecules present in the sample. The technique is therefore suitable for the volume measurements in this study. The fluorescence intensity is measured as follows. First, the skin samples injected with rhodamine B are pipetted into a microplate well. The well is placed inside a microplate reader (Figure 10). This system contains a visible light source, a detector and an excitation and emission filter. It is important to filter the visible light to retain only the excitation wavelength, 550 nm for rhodamine B. This light excites the rhodamine B molecules which consequently emit photons. These photons are filtered by an emission filter. Light with only a wavelength of 600 nm passes through the filter and is detected to calculate the number of molecules injected into the skin samples.

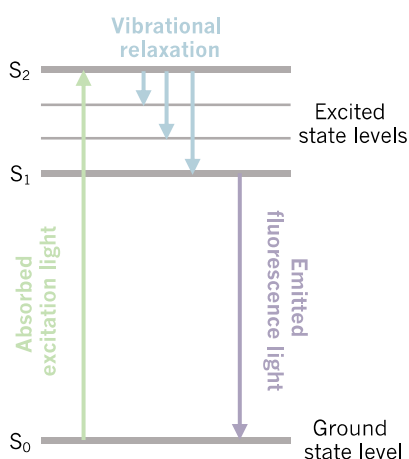


Figure 9: Jablonski diagram of fluorescence.

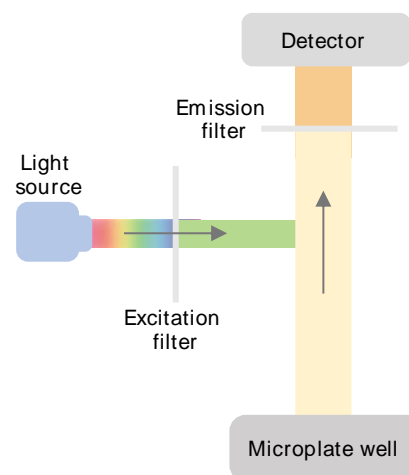


Figure 10: Illustration of the microplate reader.

The injection depth and volume measurements were first tested on porcine skin, which is widely available and easy to collect, to optimize the procedure. The final experiments were executed on *ex vivo* human skin.

### 3.2.1 Skin preparation

The experiments on *ex vivo* porcine and human skin were carried out in the research department of Mesoscale Chemical Systems at the University of Twente. Porcine skin was collected from the butcher (Slagerij Nijboer, Enschede) and preserved in Dulbecco's Modified Eagle Medium (Thermo Fisher Scientific). The porcine skin was stored frozen at  $-20^{\circ}\text{C}$ . Human skin was collected in Deventer Ziekenhuis from (prophylactic) mastectomy surgery. The clinical pathology department received the removed tissue and investigated the tumour and the surrounding skin. The residual skin was stored at  $-80^{\circ}\text{C}$  at the clinical pathology department for three months, thereafter it was free of medical purposes. Informed consent for using the residual skin was obtained by the clinical pathology department. Skin slabs from two individuals (13 x 6 and 14 x 9 cm) were collected and were suitable for the human skin experiments. The skin was transported from the hospital to the laboratory of the University of Twente in a cooling system at  $-20^{\circ}\text{C}$ .

The porcine and human skin were defrosted a few hours before the start of the experiments. The skin was shaved and secured with needles to a styrofoam plate. A strain of 10% was applied in both directions to mimic *in vivo* skin. Eight circles were marked by tape on the porcine skin: four circles for the soft pricks and four circles for the hard pricks. Three of the soft and hard pricks were used for injection depth and volume determination and one of each for histological sections. Sixteen circles were marked by a blue coloured pen on the human skin: eight circles for the soft pricks and eight circles for the hard pricks. Six of the soft and hard pricks were used for injection depth and volume determination and two of each for histological sections. The diameter of the circular marks was 4 mm and corresponds with the size of the biopsy opening.

### 3.2.2 Skin Prick Test

Histamine (Soluprick Controlevloeistoffen Positieve 100 mg/mL Histamindihydrochloride, ALK) was combined with Rhodamine B (RhoB) at a concentration of 2 mg RhoB/1 mL. Droplets of 10  $\mu\text{L}$  histamine-RhoB were pipetted on the circular marks. Soft and hard pricks were applied using the Force Gauge-lancet setup with an ALK lancet (Figure 4). A soft prick was defined as 5 g and a hard prick as 60 g (section 2.3.1). Ten seconds after the injection, the droplet was removed by a pipette and a cotton swab. After the test, the histological sections were cut and the injection depth and volume were determined.

### 3.2.3 Skin quality assessment

Biopsies of the skin were taken using the disposable Biopsy Punchers (PFM Medical, 4 mm). The skins samples were preserved in a cryomold (Seal'n Freeze Cryotray Intermediate, Ted Pella Incorporated), submerged with optimal cutting temperature compound (PolyFreeze Tissue Freezing Medium, Sigma-Aldrich), frozen in isopentane and cooled by liquid nitrogen. Thereafter, the biopsies were sliced using a cryostat at  $-16^{\circ}\text{C}$  (Leica CM1520) with a slice thickness of 10  $\mu\text{m}$  and fixated using acetone. Haematoxylin/Eosin staining (Sigma-Aldrich) was applied to visualise the anatomy of the skin. The histological sections were imaged using the Nikon Ti-E microscope and captured with the Hamamatsu C11440 Orca Flash 4.0LT camera.

### 3.2.4 Injection depth determination

OCT cross-sections of the pricking holes in the XY, XZ and YZ directions were generated to measure the injection depth. The used OCT system is custom-built at the University of Twente and is optimised for visible light in the range of 450 to 650 nm. The OCT cross-sections were analysed in Fiji (ImageJ, version 2.9.0) to find the pricking hole and select the XZ and YZ cross-sections of the maximum injection point. The cross-sections were analysed in MATLAB (2022a) to measure the injection depth. The injection depth was measured by creating a triangle between the two intact stratum corneum points and the maximum injection point. The injection depth was defined as the distance between the maximum injection point perpendicular

to the middle point of the line between the two intact stratum corneum points. An example of an injection depth measurement is illustrated in Figure 12. The script of the injection depth measurements can be found in Appendix I.

### 3.2.5 Injection volume determination

Biopsies of the pricking holes were taken using the disposable Biopsy Punchers (PFM Medical, 4 mm). Each skin sample was placed in a 2 mL bead-bug microtube with garnet shards with one zirconium bead (diameter 6.0 mm) with the addition of 1 mL RIPA buffer (RIPA Lysis and Extraction Buffer, Thermo Scientific). The microtubes were placed ten times alternating for three minutes in the BeadBug microtube homogenizer (Merck KGaA) and PCV-2400 Combined Centrifuge/Vortex Mixer (Grand Instruments). The shaking and centrifuging with garnet shards and zirconium beads in the microtubes resulted in rapid cell disruption and homogenisation of the tissues. After this process, the microtubes were centrifuged for 15 minutes to sedimentate the remaining grains. Next, 400  $\mu$ L was pipetted from the supernatant and transferred to an Eppendorf cup, containing a filter paper (Whatman 201) to remove any residual grains.

The fluorescence was measured for different histamine-RhoB concentrations to create a calibration curve. The different concentrations were obtained by diluting the original histamine-RhoB solution with the RIPA buffer. For the porcine skin experiments, the maximum concentration was 100  $\mu$ g/mL and diluted in fifteen steps to 0.001  $\mu$ g/mL. The maximum concentration in the human skin experiments was 10  $\mu$ g/mL and diluted in twelve steps to 0.0098  $\mu$ g/mL. The calibration and tissue solutions (100  $\mu$ L) were pipetted in a black microplate for fluorescence-based assays (Corning Incorporated). The VICTOR X3 Multimode plate reader (PerkinElmer) with an excitation wavelength of 555 nm and an emission wavelength of 600 nm was used to read the fluorescence signal. The fluorescence of the tissue samples was converted to injection volumes in  $\mu$ g by the equation of the calibration curve. The calibration curves were created in Excel (2022) and can be found in Appendix II.

## 3.3 Results

A total of six and twelve biopsies were taken from the porcine and human skin respectively to determine the injection depth and volume. Two porcine skin biopsy and four human skin biopsies were collected for histological sections to assess the quality of the skin samples. Due to lack of time, histological analyses were done for only one porcine and one human skins sample.

### 3.3.1 Skin quality assessment

The histological sections of the porcine and human skin sample with the corresponding OCT cross-section are displayed in Figure 11. The porcine skin was preprocessed at the butcher and the stratum corneum and epidermis were partly burned from the skin. From the histological sections of the human skin can be concluded that the epidermis and stratum corneum were intact and not destructed during transport or cooling. The stratum corneum can be recognised as the long pink structure at the surface of the skin in the histological sections and as the bright white outermost layer in the OCT cross-section. The epidermis is visible in the histological section as the dark pink layer with purple nuclei and in the OCT cross-section as the light grey layer.

### 3.3.2 OCT images

The OCT images of the third soft prick in porcine skin and the third hard prick in human skin can be found in Figure 12 as an example of the injection depth measurement. The XY cross-sections show the surface of the skin: the applied tape and coloured pen are seen as dark grey and the skin is seen as light grey/white. The red cross in the XY cross-section indicates the pricking hole. The XZ and YZ cross-sections show a triangular shaped disruption of the skin. The injection depth is visualised by the yellow line.

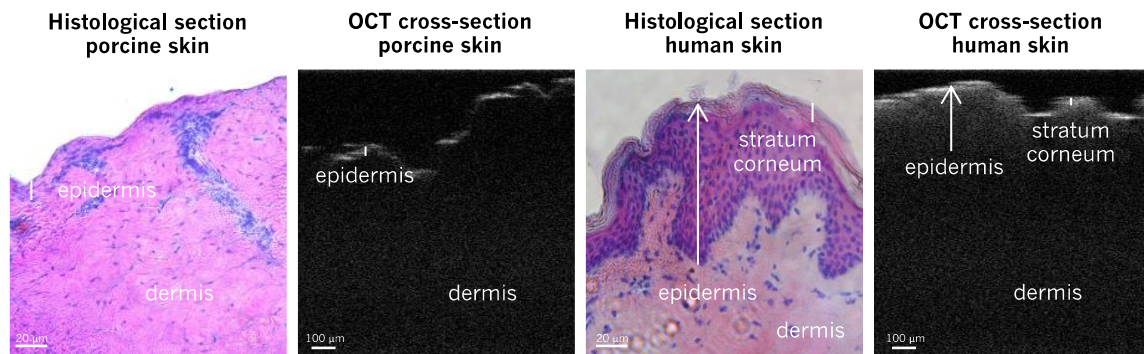


Figure 11: Histological sections of the porcine and human skin sample with the corresponding OCT cross-sections. The stratum corneum can be recognised as long pink structures at the surface of the skin in the histological sections and as the bright white outermost layer in the OCT cross-section. The epidermis is visible in the histological section as the dark pink layer with purple nuclei and in the OCT cross-section as the light grey layer.

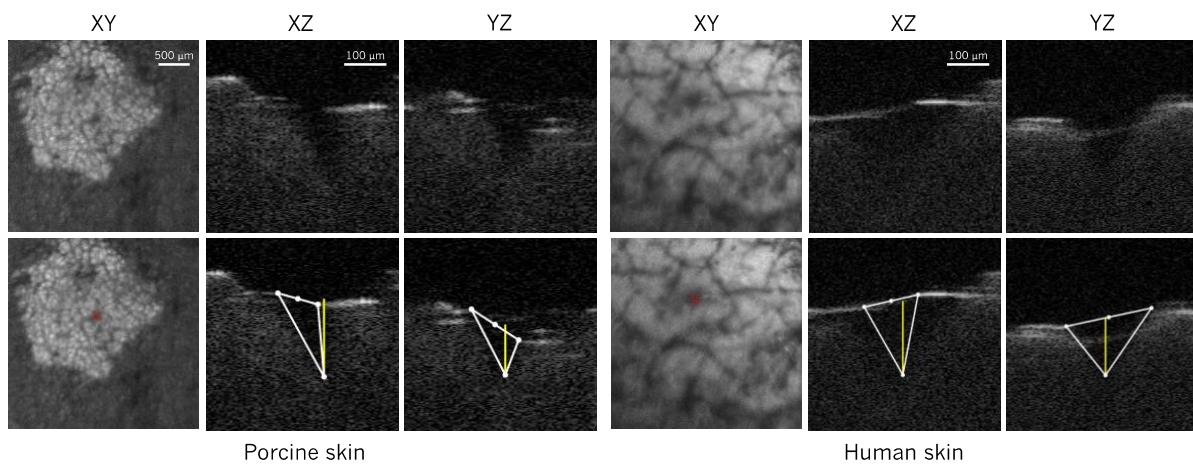


Figure 12: OCT cross-sections of the third soft prick in porcine skin and the third hard prick in human skin. The XY cross-sections show the surface of the skin and the XZ and YZ cross-sections show the triangular shaped disruption of the skin. The red cross indicates the pricking hole and the yellow line shows the injection depth. The scale of 500  $\mu\text{m}$  applies to the XY cross-sections and the scale of 100  $\mu\text{m}$  applies to the XZ and YZ cross-sections.

### 3.3.3 Injection depth and volume

Table 2 provides an overview of the injection depths with corresponding injection volumes of the soft and hard pricks in porcine and human skin. The mean injection depth in porcine and human skin of a soft prick was respectively 173  $\mu\text{g}$  and 117  $\mu\text{g}$  of a hard prick 189  $\mu\text{g}$  and 158  $\mu\text{g}$ .

Two scatter plots of the relation between the injection depth and volume in porcine skin and human skin are presented in Figures 13 and 14. The scatter plot of the porcine skin shows a low correlation between injection volume and injection depth ( $R^2 = 0.04$ ). The scatter plot of human skin reveals contradictory results: an increase in injection depths causes an increase in injection volumes ( $R^2 = 0.24$ ).

Table 2: The injection depth in  $\mu\text{m}$  and the injection volume in  $\mu\text{g}$  of the soft and hard pricks.

PORCINE SKIN				
Soft prick			Hard prick	
	Injection depth ( $\mu\text{m}$ )	Injection volume ( $\mu\text{g}$ )	Injection depth ( $\mu\text{m}$ )	Injection volume ( $\mu\text{g}$ )
1	243	0.141	234	0.134
2	152	0.195	143	0.119
3	126	0.255	191	0.394
HUMAN SKIN				
Soft prick			Hard prick	
	Injection depth ( $\mu\text{m}$ )	Injection volume ( $\mu\text{g}$ )	Injection depth ( $\mu\text{m}$ )	Injection volume ( $\mu\text{g}$ )
1	120	0.073	126	0.060
2	181	0.236	205	0.106
3	138	0.131	173	0.327
4	82	0.081	155	0.104
5	82	0.111	166	0.138
6	98	0.090	123	0.178

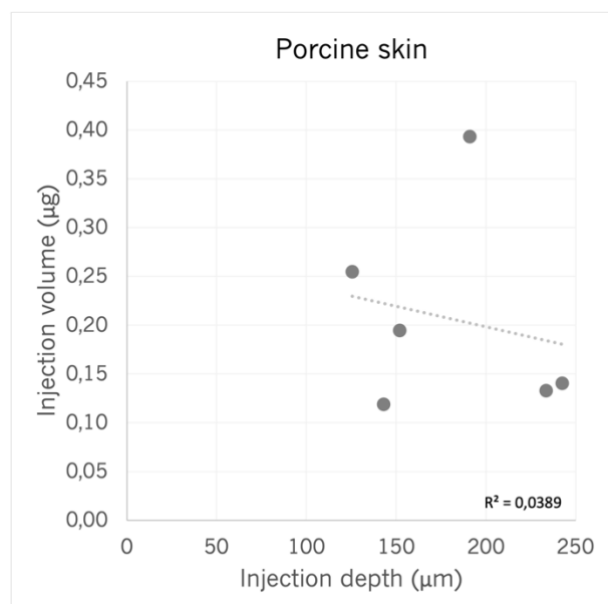


Figure 13: Scatter plot of the correlation between injection depth and injection volume in porcine skin.

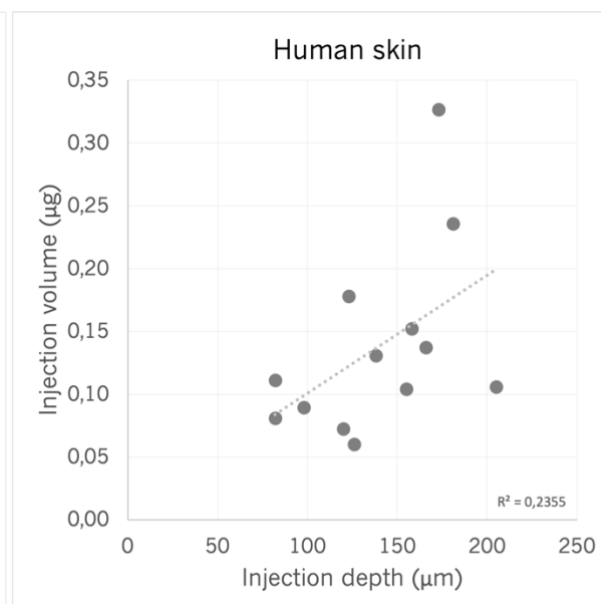


Figure 14: Scatter plot of the correlation between injection depth and injection volume in human skin.

## 3.4 Discussion

### 3.4.1 Results

The present study was designed to explore the relation between the injection depth and injection volume in the SPT. The results of the injection depth measurements in the porcine and human experiments show a lower injection depth (mean between 117 and 189  $\mu\text{g}$ ) compared to the estimations in literature (between 2 and 3 mm). The estimations in literature are based on the size of the lancet tip and are less accurate compared to the measurements on the OCT cross-sections. The results of the volume measurements in porcine and human skin show contradictory outcomes. The results of the porcine skin experiments show a decline in injection volume with an increase in injection depth. This finding was unexpected and is not in line with the hypothesis. The human skin experiments suggest that an increase in injection depth will result in a higher injection volume. This can be explained by the fact that more liquid can enter the skin due to the larger skin interruption. The discrepancy between the porcine and human skin results could be attributed to the performance quality of the experiments. The porcine skin experiments were executed to test and fine-tune the procedure and could therefore be less reliable compared to the procedure of the human skin experiments. For example, the porcine skin was not dried before the experiments, and the histamine droplet spread out on the skin surface. During the human skin experiments, the skin was first dried and the histamine droplets remained intact on the skin surface. In addition, the stratum corneum and the dermis were partly burned from the porcine skin while the human skin was intact. One important function of the stratum corneum is to retain water and hydrate the skin and could therefore contribute to the absorption of the injected liquid. The absorbed volume could therefore differ between the porcine and human skin. Furthermore, a closer inspection of the porcine and human skin scatter plots show that the distribution of the points is rather random ( $R^2 = 0.04$  in porcine skin and  $R^2 = 0.24$  in human skin). Conclusions cannot be drawn from these experiments because the correlation coefficients are very low and further research is necessary to confirm or reject the hypothesis. If the hypothesis is correct, this could mean in clinical context that different volumes of allergen extracts enter the skin because the medical assistants show a high intra- and inter-operator variability (Chapter 2). The sensitisation reaction could increase when a larger amount of volume is injected which could lead to a variation in wheal sizes. The latter will be investigated in Chapter 4.

### 3.4.2 Limitations

Several limitations need to be noted regarding the porcine and human skin experiments. The first limitation was the sample size: only six porcine skin samples and twelve human skin samples were included. Due to lack of time and resources, it was not possible to optimise the procedure further using porcine skin and repeat the experiments in human skin to expand the dataset. The second limitation was the destructed skin surface of the porcine skin samples. These skin samples were therefore not a true representation of the skin and could respond differently to the applied SPT compared to the intact skin samples. The third limitation of the study was the assessment of the OCT cross-sections. The pricking hole was selected on the XY cross-sections but sometimes it was difficult to distinguish the pricking hole from skin folds or hair follicles. In addition, a few OCT cross-sections were blurred because the skin samples were not exactly aligned with the focus of the beam in the OCT system which complicated the selection of the pricking holes. In these cases, a second researcher assessed the OCT cross-sections to minimize the risk of selection errors. Another source of uncertainty was the possibility of injection volume measurement errors. The human skin experiments took place 25 days after the porcine skin experiments and in these days RhoB sediment was formed in the histamine-RhoB solution. The assumption was made that the solution was saturated and that the sediment formation did not affect the results. Therefore, the sediment was filtered from the histamine-RhoB solution prior to the human skin experiments to create a clear solution. Furthermore, it was difficult to homogenate the skin sample, especially in the presence of a subcutaneous fat layer. In these cases, not all fat particles could be filtered which could disturb the fluorescence signal. This occurred mostly during the porcine skin experiments.

### 3.4.3 Future recommendations

Further work is required to validate the findings of this study. The first recommendation is to include more porcine and human skin samples to optimize the procedure of the injection depth and volume measurements and to expand the data set. Furthermore, various mark materials could be investigated to find a convenient marker that is easy to apply on the skin samples and generates a high contrast on the OCT images. Another recommendation is to evaluate the OCT protocol in detail to increase the quality of the OCT cross-sections and the reliability of the pricking hole selection. Moreover, the fluorescence signal is prone to be influenced by a variety of factors and could therefore affect the injection volume results. Consequently, alternative volume measurement methods could be considered that can detect a small amount of injection material for example by using radioactive molecules as written in the review of Roseboom *et al.*<sup>54</sup>

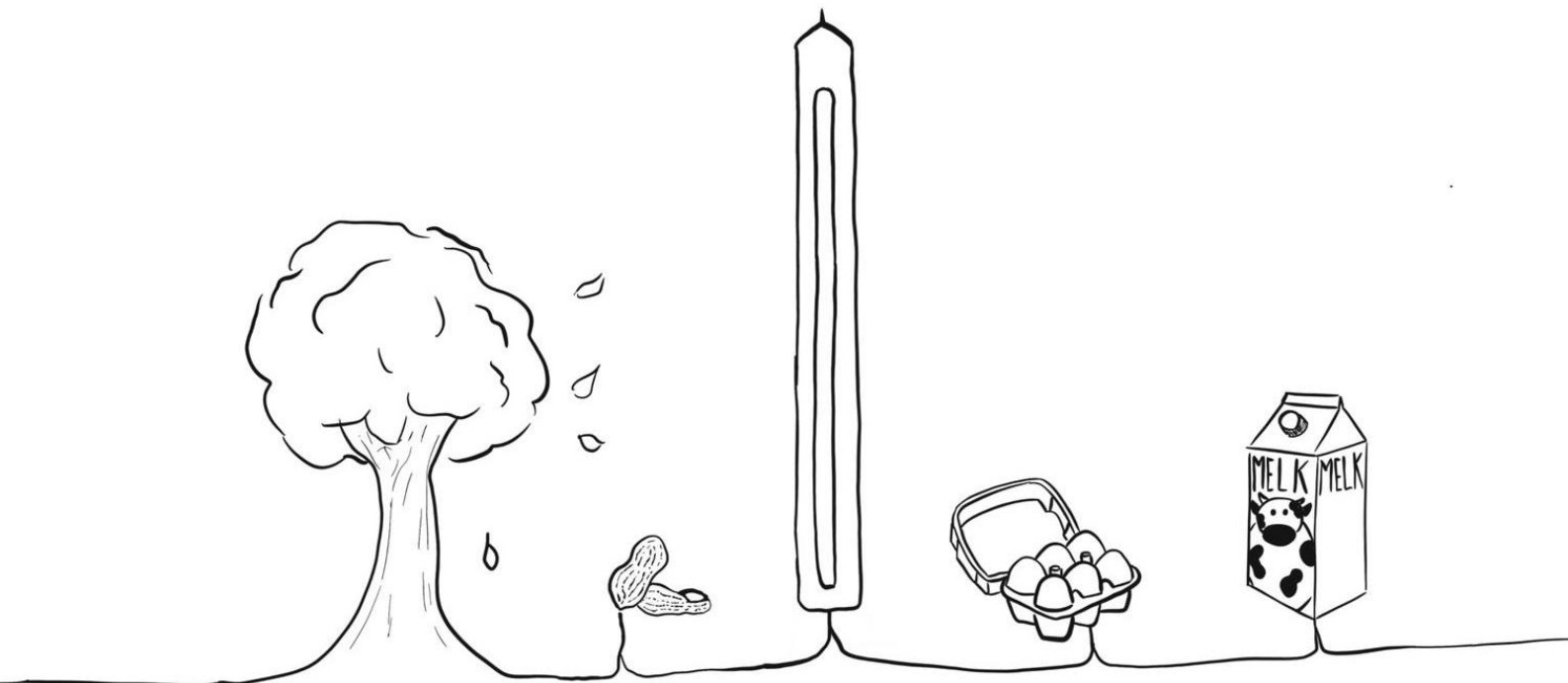
## 3.5 Conclusion

This is the first study investigating the relation between the injection depth and volume in the SPT in porcine and human skin using a lancet. The injection depth was measured on OCT cross-sections and histamine was labeled with fluorescence molecules to determine the injection volume. The results of the porcine and human skin experiments show contradictory results and a low correlation between the injection depth and injection volume was found. Although conclusions cannot be drawn due to the contradictory results and small sample size, this research lays the groundwork for future studies. Further research should focus on optimising the OCT protocol and explore alternatives for accurate injection volume determination.

# Chapter 4

## *Phase II:*

The relation between the injection depth and wheal size in healthy subjects



## 4.1 Introduction

The previous chapter described the study towards the relation between the injection depth and injection volume in the SPT. This chapter provides insight into the effect of the injection depth on the wheal size. There are a large number of published studies that measured the wheal size to compare different SPT devices but there is a current paucity of scientific research quantifying the effect of the injection depth on the wheal size.<sup>26,27,30,55</sup> Previous studies recognised the influence of the amount of trauma imparted to the skin on the wheal size but in-depth research is missing.<sup>27,29</sup> Therefore, the study presented in this chapter is one of the first investigations to examine in detail the relation between the injection depth and wheal size in healthy volunteers.

The initial plan was to measure the injection depth using OCT as described in the previous chapter. The OCT system at the University of Twente was used during the test measurements for this study but was not available for the main measurements due to lack of time and resources. The OCT system at the ophthalmology department in Deventer Hospital was taken into consideration but the resolution was not sufficient to visualise the upper layers of the epidermis. For this reason, the decision has been made to compare the effect of the soft and hard pricks (section 2.3.1) on the wheal size instead of measuring the exact injection depth. The hypothesis states that the hard pricks will induce a larger wheal compared to the soft pricks.

## 4.2 Method

In this part of the study, the wheal size was measured to compare the soft and hard pricks. In previous studies, the wheal size was determined by measuring the mean wheal diameter which is the average of the longest orthogonal diameters.<sup>26,27,30,55</sup> This approach is based on the assumption that the surface of the emerging wheals has a circular or ellipsoidal shape. The surface of these shapes is calculated by the following equations:

$$\textit{Surface circle} = \pi * \textit{radius}^2 \quad (2)$$

$$\textit{Surface ellipse} = \pi * \textit{horizontal radius} * \textit{vertical radius} \quad (3)$$

However, the wheals often have an irregular contour in clinical practice and the orthogonal diameters alone are inadequate to calculate the wheal surface. For this reason, the wheal surface will be calculated to compare the soft and hard pricks and the wheal diameter is automatically determined to compare the findings to literature.

The study in healthy volunteers was executed in Deventer Hospital. Colleagues and fellow students who were interested to participate in this pilot study could sign up voluntarily. The inclusion criterion was age > 18 and the exclusion criteria were the use of antihistamines and/or corticosteroids and suffering from a skin disorder. Enrolment of volunteers for the study occurred between the 15<sup>th</sup> of December 2022 and the 19<sup>th</sup> of January 2023. All obtained data were processed anonymously.

### 4.2.1 Skin Prick Test

The SPT was executed according to the protocol applied in Deventer Hospital.<sup>56</sup> The test was executed on the volar aspect of the left and right forearm. Eight histamine droplets of 10 mL (Soluprick Controlevloeistoffen Positieve 10 mg/mL Histamindihydrochloride, ALK) were pipetted on each arm and pricked into the skin using the Force Gauge-lancet setup with an ALK lancet (Figure 4). The droplets were placed alternately on the lateral and medial aspects of the forearm taking hairs and tattoos into account. The lancet was pressed through the histamine droplet perpendicular in the skin. Four droplets per arm were

pricked into the skin by a soft prick (5 g) and the other four droplets by a hard prick (60 g). The droplets were removed from the arm ten seconds after the injection. An ArUco marker was placed proximally on the forearm to calculate the pixel size afterward. After ten minutes, the emerging wheals were captured using an iPhone camera (SE 2020, Apple). The images were taken parallel to the forearm and as close to the forearm as possible taking the wheals and ArUco marker into account. A video of the wheals was made as an additional tool for wheal segmentation. After the test, Betnelan (1mg/g, GSK) was applied on the forearm to reduce itching.

## 4.2.2 Wheal size

The images of the forearms were edited in Preview (Apple); the intensity of the red colour in the images was increased and the contrast was adjusted to increase the visibility of the wheals. The wheals were then cropped and manually segmented in Paint 3D (2022). The videos of the wheals were used to distinguish the wheal from the surrounding flare. The segmentations were converted to binary images in MATLAB (2022a) and the pixel size was determined using the size of the ArUco marker. Pixel counting was applied to determine the wheal size. The mean wheal diameter was also automatically determined on the binary wheal images to compare the findings to literature. The mean diameter of the wheal is the average of the longest orthogonal diameters. All SPTs and wheal segmentations were executed by one researcher. The script of the wheal size and diameter measurements can be found in Appendix III and an overview of the segmentation steps can be found in Appendix IV.

## 4.2.3 Statistical analysis

Statistical analyses were performed to investigate if there was a significant difference in wheal size between the soft and hard pricks. The data were first assessed to be normally distributed by visual inspection of the histograms. If the data were normally distributed, a paired samples T-test was conducted. If the data were non-normally distributed, the Wilcoxon signed-rank test was performed. A  $p$  value of  $<0.05$  was considered significant. The data were analysed in IBM SPSS Statistics 26.

The sensitivity of the SPT was determined by the number of reliable histamine wheals which were the histamine wheals with a diameter  $> 3$  mm. Sensitivity was calculated by the following equation:

$$\text{Sensitivity} = \frac{\text{number of wheals with diameter } > 3 \text{ mm}}{\text{number of wheals measured}} \quad (4)$$

## 4.2.4 Test measurement

A test measurement was performed at the University of Twente to test the aforementioned method. A soft and hard prick was performed on one healthy volunteer. The soft and hard pricks were not controlled by the Force Gauge-lancet setup but manually set. After the injections, the pricking hole was imaged by the OCT system and the injection depth was measured according to the method described in section 3.2.4. The two emerging wheals were captured by an iPhone (SE 2020, Apple) and manually segmented to determine the wheal size as mentioned in section 4.2.2. Statistical analysis was not performed because only one healthy volunteers was included to test the method.

## 4.3 Results

Twenty-one healthy volunteers were recruited for this study. In total, 168 hard pricks and 168 soft pricks were performed.

The boxplot in Figure 15 shows the distribution of the wheal sizes induced by a soft and hard prick. The cross in the boxplot indicates the mean value. The green boxplot shows the distribution of the soft pricks and the blue boxplot the distribution of the hard pricks. The mean wheal size for a soft and hard prick was

respectively 3.98 mm<sup>2</sup> (standard deviation of 2.59 mm<sup>2</sup>) and 5.82 mm<sup>2</sup> (standard deviation of 2.42 mm<sup>2</sup>). The data were normally distributed and a paired samples T-test revealed a significant difference between the wheal sizes induced by a soft and hard prick ( $p < 0.001$ ).

The mean wheal diameter for a soft and hard prick was respectively 2.23 mm (standard deviation of 0.71 mm) and 2.81 mm (standard deviation of 0.62 mm). The sensitivity of the SPT was for the soft pricks 15.5% and for the hard pricks 42.9%.

The test measurement showed for the soft prick a wheal size of 14.2 mm<sup>2</sup> with an injection depth of 77 μm. The results of the hard prick showed a wheal size of 18.7 mm<sup>2</sup> and an injection depth of 114 μm.

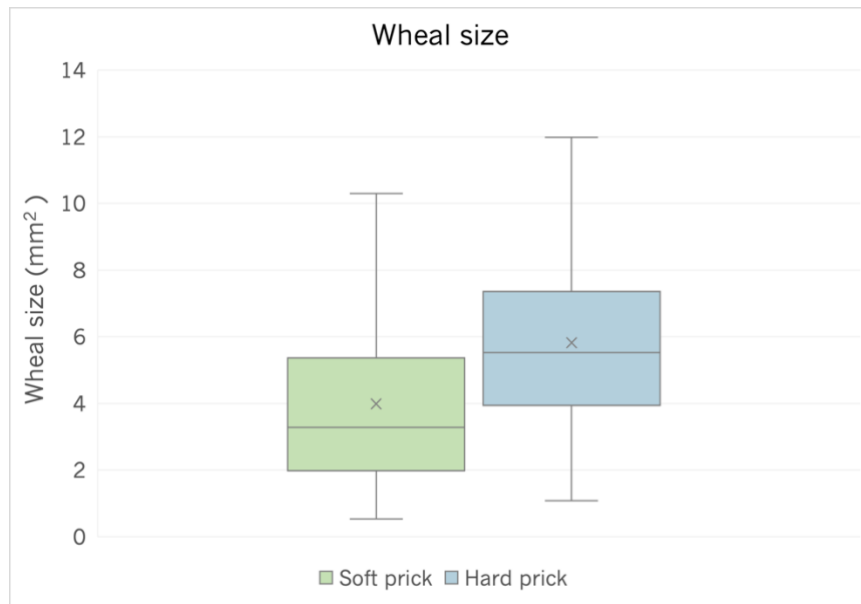


Figure 15: Comparison of the wheal sizes induced by a soft (green) and hard (blue) prick. The grey cross indicates the mean value.

## 4.4 Discussion

### 4.4.1 Results

The study in healthy volunteers aimed to investigate how the injection depth was related to the wheal size in the SPT. The first important finding was the large range in wheal sizes of both the soft and hard prick although the injection depth was controlled by the Force Gauge-lancet setup. A previous study evaluated the variations in wheal size by calculating the coefficient of variation and reported a variation between 20% and 40% using a lancet.<sup>20</sup> A possible explanation may be that the sensitivity of the skin differs. Prior SPT studies have shown that the sensitivity differs between the back and forearm and Janssens *et al.* showed a significantly higher mast cell density in the upper arm compared to the forearm.<sup>57-59</sup> These findings suggest the possibility that the sensitivity could also differ between locations on the forearm which could affect the wheal size. Despite the large range, statistical analysis showed a significant difference between the wheal sizes induced by a soft and hard prick. A hard prick induces a larger wheal (mean of 5.82 mm<sup>2</sup>) compared to a soft prick (mean of 3.98 mm<sup>2</sup>). The present study only compared the soft and hard pricks and did not take the exact injection depth into account. However, the injection depth was determined during the test measurements and the results showed an increase in wheal size of approximately 24% with an increase in injection depth of approximately 26%. The results of the present study and test measurement support the idea that the wheal size is affected by the injection depth. This has consequences in clinical practice because the injection depth is not standardised and the extracts could be pricked into the skin at different depths.

In these situations, the wheal size does not only depend on the level of sensitisation but also on the SPT performance.

To compare the wheal sizes to literature, the mean wheal diameter was calculated for the soft (mean of 2.23 mm) and hard (mean of 2.81 mm) pricks. These findings were contrary to previous studies which suggested that the mean wheal diameter was between 3.8 and 5.45 mm using a lancet.<sup>22,23,26,27</sup> Also the sensitivity reported in these studies were higher (between the 93.2 and 100%) compared to sensitivities calculated in this study (15.5% for soft pricks and 42.9% for the hard pricks). The discrepancy in diameter may be due to the manually measurements in the previous studies which were sensitive to errors because different size markers were used and the diameters were determined and measured manually using a ruler.<sup>60</sup> The differences in sensitivity can be explained by the fact that the cut-off value is based on manually measurements and is not validated for automatically measurements. The sensitivity for the soft pricks were also lower compared to the sensitivity of the hard pricks. In clinical practice, this could lead to a higher number of unreliable SPTs when the medical assistants injected the histamine droplet softly into the skin.

#### 4.4.2 Limitations

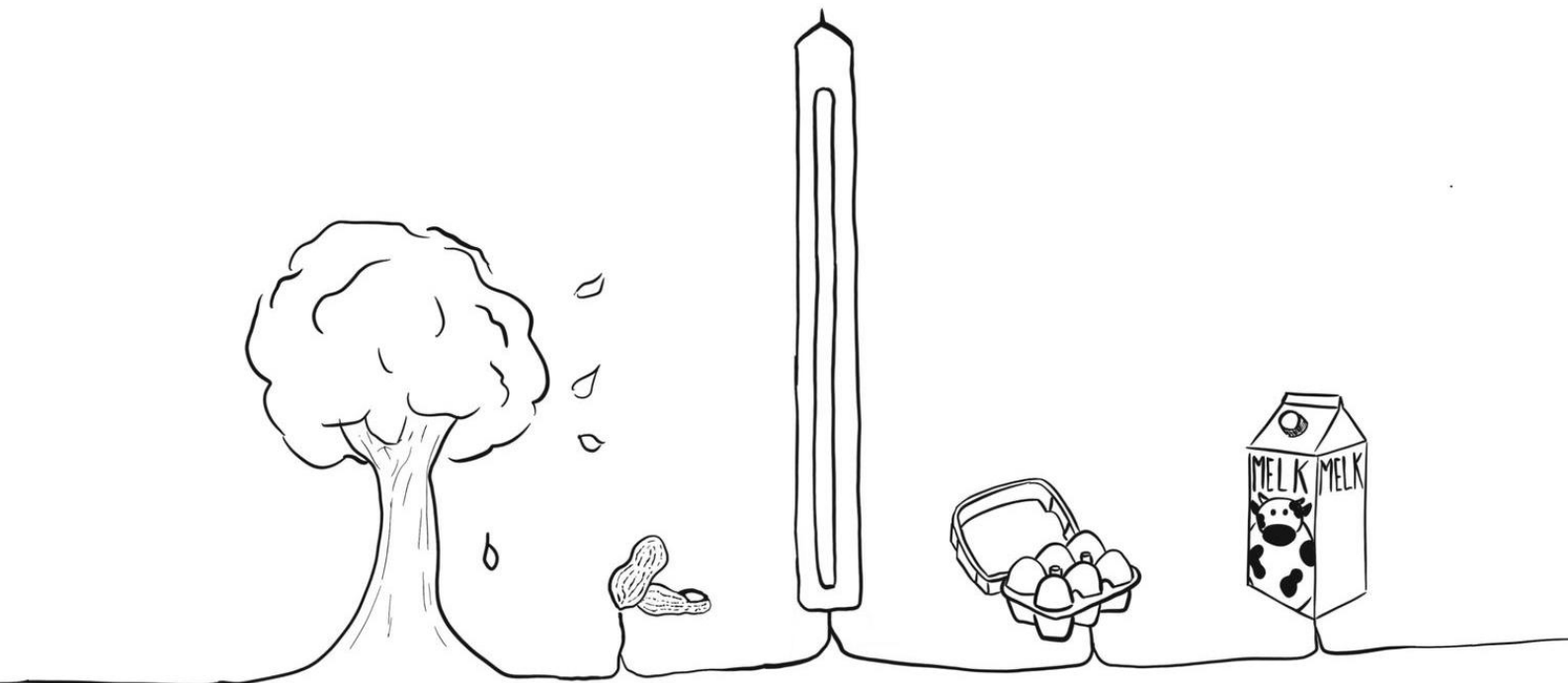
Several limitations to this study need to be acknowledged. First, this study only included healthy volunteers and it is possible that the results may not be generalisable to allergic adults or children. In addition, only histamine was tested but it would be interesting to repeat the experiments with allergen extracts. Secondly, it was not possible to assess the exact injection depth; therefore, it is unknown which injection depth corresponds to a soft and hard prick. The soft and hard pricks were controlled by the Force Gauge-lancet setup but small measurement errors could occur during pricking. Further research could validate the soft and hard prick by imaging the pricking hole to gain more knowledge about the exact injection depth and the relation between the injection depth and wheal size. The last limitation was the paired samples T-test which did not correct for the fact that every eight wheals derived from the same volunteer within the soft and hard prick group. Other statistical tests that correct for all the paired samples could be explored, although it is not expected that this would lead to different results because of highly significant findings.

#### 4.5 Conclusion

This is the first study that investigated the effect of the injection depth on the wheal size in the SPT in healthy volunteers. Soft and hard pricks were performed using the Force Gauge-lancet setup and the wheals were captured and manually segmented to calculate the wheal size. The results of the study show a significant difference between the wheal size induced by a soft and hard prick. This finding could have clinical consequences because the injection depth is not standardised in the SPT causing the wheal size to depend on the SPT performance. Further research should focus on the validation of the injection depth of the soft and hard pricks by imaging the pricking hole to gain more knowledge about the exact injection depth and the relation between the injection depth and wheal size.

# Chapter 5

Needle-free injection as  
future perspective in the  
Skin Prick Test



The initial goal of this thesis was to explore lancet alternatives to increase the reproducibility of SPT performance. As stated before, the SPT performance can be affected by a variety of factors, such as different puncture tips, the amount of pressure applied on the device and the angle of application.<sup>20</sup> A novel device that could improve the SPT performance is the microjet injector, which is being developed and studied in the research department of Mesoscale Chemical Systems at the University of Twente. The study focused on investigating the possibilities of injecting allergen extracts into the epidermis using the microjet injector. During the test experiments, it was concluded that this technology was not sufficient to perform allergen injections in *ex vivo* skin. The aim of the thesis was adjusted to the previously described fundamental SPT study. However, the first results of the microjet injection experiments could be considered in future research and are therefore elaborated in this chapter.

## 5.1 Introduction

The first needle-free injector was invented in 1866 and over the past years, several mechanical- and gas-powered models were developed and commercialised. However, the World Health Organization banned the needle-free injector from the market due to cross-contamination caused by splash-back of the injected liquids. In the 21<sup>st</sup> century, laser-based microjet injectors were developed and investigated. The laser energy, beam diameter, and filling level of the liquid chamber can be adjusted to control the injection depth and volume for personalised medicine which is an advantage with respect to the needle-free injectors in the past.<sup>20</sup> Other advantages are the reduction of pain and medical waste, and this device could be the solution for patients suffering from needle phobia.<sup>20,61</sup> Current research focusses on jet stability, thermo-degradation of injected compounds, jet velocity, delivered volume and splash-back to improve the injection quality.<sup>62,63</sup> Laser-based microjet injectors are mainly tested on gel substrates, *ex vivo* porcine and human skin. The next step is to explore the clinical possibilities which starts with the application of microjet injectors in the SPT.

During the SPT, droplets of allergen extracts are pricked into the epidermis with a lancet. To replace the lancet with the microjet injector, two setups are possible: 1) the allergen extract is placed inside the chamber and injected directly or 2) the microfluidic jet forces the allergen extract droplet into the skin. The first option is widely investigated in gel substrates and *ex vivo* skin and shows great potential for the future. The second option is not investigated yet but would be more desirable for the SPT because the chamber does not have to be replaced for each allergen extract during the test. This experiment aims to compare the two injection set ups and to evaluate if the microjet injector is a convenient tool in the SPT.

## 5.2 Method

The laser-based microjet injector consists of a laser, microscopic objective and an injection chamber. The laser generates a laser beam which is focussed by the microscopic objective on the injection chamber. The injector can contain two types of lasers: pulsed laser or continuous wave laser. A pulsed laser can deliver energies of 100  $\mu$ J to 1 J within femto- to microseconds. A high power will cause optical breakdown which results in an electrically conducting medium and the formation of a plasma. The energy of the laser will be absorbed by the plasma and the explosive bubble is created. The threshold for optical breakdown to occur increases with pulse duration and ultra-short pulsed lasers are therefore desirable but very expensive. Continuous wave lasers have a lower power compared to pulsed lasers and optical breakdown does not occur. The liquid is heated by the energy of the continuous wave laser which results in an explosive bubble, known as thermocavitation. This bubble displaces the liquid and a microfluidic jet is formed which can penetrate the skin without the use of a needle. A dye is added to the liquid to match the laser wavelength and the liquid to increase the absorption coefficient and optimise the absorption.<sup>62</sup>

Important characteristics of the laser-based microjet injector are jet velocity, injection depth, jet volume, jet stability and liquid temperature. A high jet velocity is imperative for effective skin injections and the velocity is enhanced by a narrow chamber width, low chamber filling level and the implementation of a tapered nozzle within the chamber.<sup>64,65</sup> The injection depth reported in literature ranged between 100 and 2000  $\mu\text{m}$  depending on the substrate and the number of jet injections.<sup>62</sup> Research showed that the injection depth reached a maximum after 20 jet injections in hydrogel and 150 jet injections in porcine skin.<sup>66,67</sup> The challenge in determining the corresponding injection volume arises from the three-dimensional volume measurement on a two-dimensional image which resulted in a lack of mention of injection volumes in most studies. Jet stability is also a frequently investigated characteristic because it is important to preserve a stable jet until impact because an instable jet results in a smaller penetration depth and splash-back. At last, the laser can heat the liquid to a maximum temperature of 98° and it is unclear what the impact of heating is on the efficacy of active compounds present in pharmaceutical products.<sup>62</sup>

## 5.2.1 Experiments

The experiments were carried out in the research department of Mesoscale Chemical Systems at the University of Twente. Two experiments were performed: 1) the red dye simulated the allergen extract and was injected directly from the chamber into the agarose gel and 2) a droplet of green dye simulated the allergen extract, was placed on the agarose gel and was injected indirectly by the force of the red dye microfluidic jet (Figure 16A). The first experiment was repeated 21 times. The second experiment was conducted 9, 5 and 5 times with respectively a droplet of 3  $\mu\text{l}$ , 15  $\mu\text{l}$  and 20  $\mu\text{l}$ .

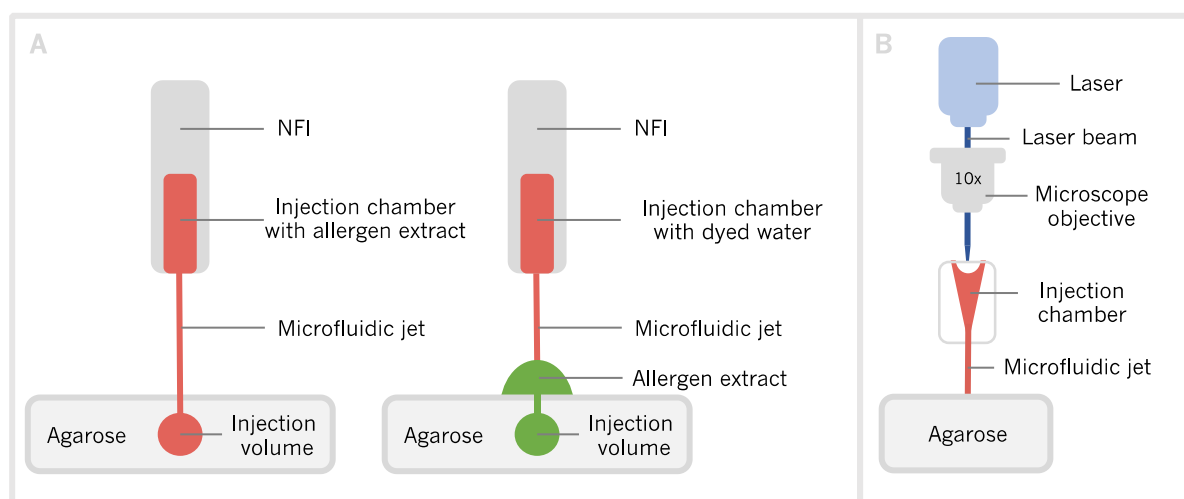


Figure 16: A) On the left image, the allergen extract is directly injected into the skin using a microfluidic jet created by thermocavitation. On the right image, the allergen extract is placed onto the skin and injected by the force of the microfluidic jet. B) Schematic overview of the needle-free microjet injector. The microscope objective focusses the laser beam on the chamber. The liquid in the chamber absorbs the optical energy, resulting in a fast-growing explosive bubble. This bubble displaces the liquid and a microfluidic jet is formed which can penetrate the agarose.

The needle-free microjet injector based on thermocavitation was used as injection device. A continuous-wave laser diode ( $P = 3.5 \text{ W}$  and  $\lambda = 450 \text{ nm}$ ) was aligned with the chamber and was focused using a  $\times 10$  microscope objective. The chamber was filled with a red dye at 0.5 wt. % (Direct Red 81, Sigma, CAS: 2610-11-9) in deionised water. The red dye was used to optimize the energy absorption from the laser. The laser was switched on for 10 ms (5.8 V and 0.031 A) and the liquid was heated above its boiling point and an explosive bubble was created. A schematic overview of the microjet injector can be found in Figure 16B. This bubble pushed the liquid out of the chamber forming a microfluidic jet. Agarose 0.25 wt. % (Sigma, CAS: 9012-36-6) was pipetted into a mold, two transparent glass plates, to form a hydrogel slab of 3.4 x 1.8 x 0.9 cm. A high-speed camera (Photron FASTCAM NOVA S6 800K-C-8GB) was simultaneously triggered with the laser by Arduino to visualize the injection at 20 - 32 x 10<sup>3</sup> fps with additional illumination from a LED light source (SCHOTT). A coloured glass filter ( $\lambda = 450 \text{ nm}$ ) protected the camera from the laser light.

Images were captured with a pixel size of 10 or 17  $\mu\text{m}$  and a field of view of 256 x 896, 256 x 864 or 256 x 768. Green dyed deionised water (Green Dragon, Eternal Tattoo Supply) simulated the allergen extract droplet in the second experiment. A small hollow circular plastic object was placed on the agarose surface and the green dye was pipetted in the middle of the circular object to retain the shape of the droplet.

## 5.2.2 Data acquisition

The following variables were obtained from the high-speed camera videos: chamber filling level pre injection, injection depth, the stand-off distance between the injection chamber and agarose gel and the velocity of the microfluidic jet (Figure 17). The relationship between the chamber filling level pre injection and microfluidic jet velocity is described in literature and measured in this study to compare the findings. The injection depth is determined to compare the efficacy of the direct injection to the indirect injection. The stand-off distance is measured to verify if all injection were executed in a similar setting.

The chamber filling level pre injection was measured on the last frame before injection of the high-speed camera videos. These frames were first pre-processed in PFV4. The Look-Up Table gain was increased to enhance the contrast between the red dye in the chamber and the background. The red dye was segmented using the Magic Select tool in Paint 3D (2022). The segmentations were converted to binary images in MATLAB (2022a) and pixel counting was applied to calculate the chamber filling levels in nL. The injection depth was determined in the last frame of the high-speed camera video. The injection depth was defined from the agarose surface to the deepest injection point and was measured using the Measurement tool in PFV4 in mm. The stand-off distance between the chamber and agarose gel was measured using the Measurement tool in PFV4 in mm. The velocity of the microfluidic jet was calculated between two consecutive frames when the tip of the jet was visible in the space between the chamber and the agarose gel. The distance between the tips was divided by the time between the two frames to calculate the velocity in m/s. The velocity was calculated in PFV4.

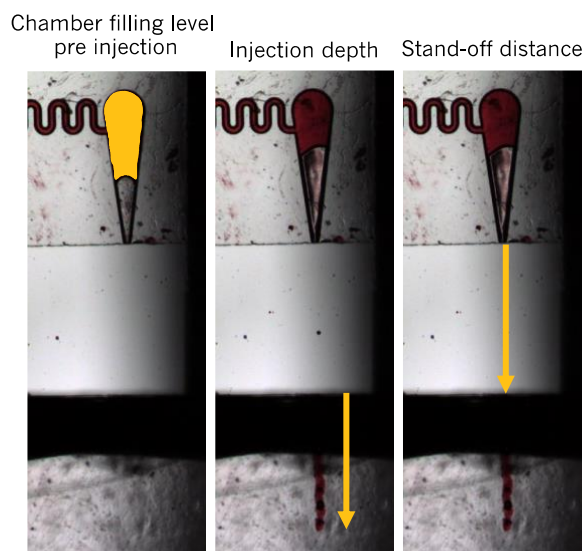


Figure 17: The chamber filling level pre injection, injection depth, and the space between the injection chamber and agarose gel are highlighted in yellow on the high-speed camera frames.

## 5.2.3 Data analysis

The aforementioned variables were analysed in Excel (2022). The dataset was too small to perform statistical tests, therefore the data was visualised in boxplots and scatter plots and described in detail to highlight potential differences between the two experimental setups.

## 5.3 Results

The following injections of the two experimental setups were included:

- Direct injection: 15 injections
- Indirect injections: 6 injections with a droplet of 3  $\mu\text{L}$  and 5 injections with a droplet of 20  $\mu\text{L}$

Two direct injections, five (droplet size = 15  $\mu\text{L}$ ) and three (droplet size = 3  $\mu\text{L}$ ) indirect injections were excluded because the tip of the jet was not visible in the space between the chamber and agarose gel and the velocity of the microfluidic jet could not be measured. Four direct injections were excluded because the injection in the agarose gel was not visible due to shadowing at the air-to-agarose transition.

### 5.3.1 Timelapse

A timelapse of direct and indirect microjet injections are respectively shown in Figures 18 and 19. Different phases of the microjet injection can be highlighted. First, an explosive bubble was created ( $t = 100 \mu\text{s}$  and  $t = 69 \mu\text{s}$ ) which built up the pressure in the chamber and pushed the red dyed water into the air space ( $t = 150 \mu\text{s}$  and  $t = 104 \mu\text{s}$ ). Subsequently, the microfluidic jet entered the top of the agarose gel or the green droplet and penetrated the gel ( $t = 250 \mu\text{s}$  and  $t = 174 \mu\text{s}$ ). The trailing part of the jet broke up ( $t = 550 \mu\text{s}$  and  $t = 451 \mu\text{s}$ ) and the injection was completed when the last drop of red dyed water contacted the agarose gel. Several dense red spots were visible within the injection site of the direct injection ( $t = 950 \mu\text{s}$ ). The injection site of the indirect injection showed a dark blob which could comprise the red and/or green dyed water.

During the indirect injection, splash-back was observed directly when the microfluidic jet contacted the green droplet. At the air-to-agarose transition, where the splashing occurred, the red microfluidic jet and green droplet cannot be distinguished due to shadowing. Therefore, it is uncertain which liquid splashes back.

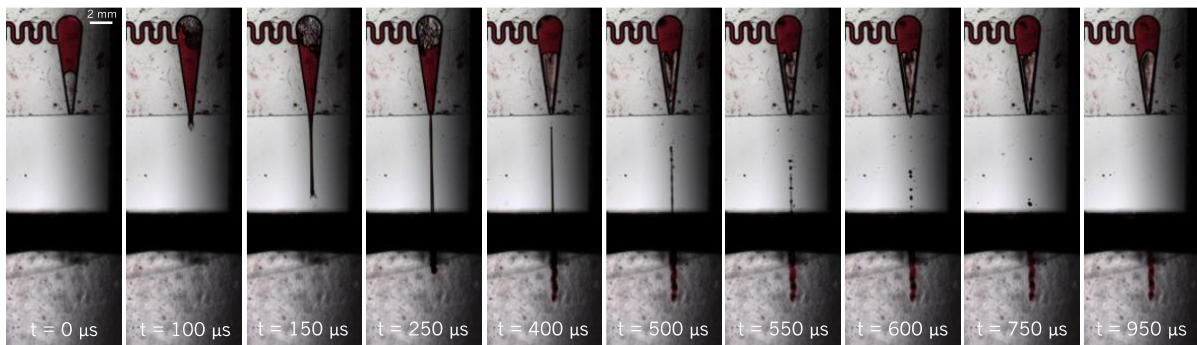


Figure 18: Timelapse of a direct microjet injection of red dye into an agarose gel recorded with the high-speed camera. The shutter speed of the camera was  $1/40000000$  s. The field of view is  $256 \times 864$  pixels with a pixel size of  $10 \mu\text{m}$ . The microfluidic jet velocity is  $31.8$  m/s.

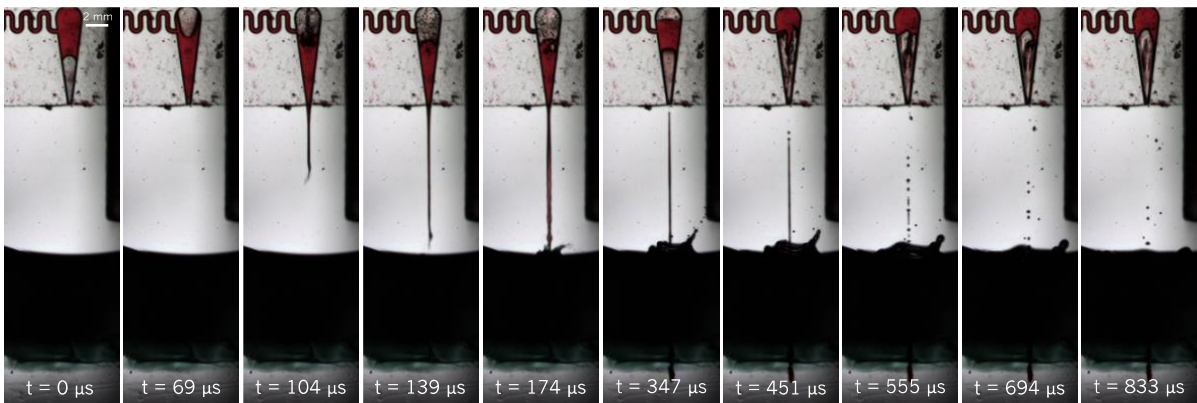


Figure 19: Timelapse of an indirect microjet injection of red dye onto a green droplet pipetted on an agarose gel recorded with the high-speed camera. The shutter speed of the camera is  $1/40000000$  s. The field of view is  $256 \times 896$  pixels with a pixel size of  $10 \mu\text{m}$ . The microfluidic jet velocity is  $43.8$  m/s.

### 5.3.2 Mean and range

Table 3 summarises the measured variables in the high-speed camera images of the direct and indirect injections. The mean and range values of the stand-off distance, chamber filling level pre injection, microfluidic jet velocity and injection depth were calculated.

Table 3: Mean and range values of the stand-off distance, difference in injection filling level, microfluidic jet velocity and injection depth measured in both experimental set-ups.

	Stand-off distance mean [range] in mm	Filling level pre injection mean [range] in nl	Jet velocity mean [range] in m/s	Injection depth mean [range] in mm
<b>Experiment 1</b>				
Injected directly	2.8 [2.1-3.6]	64.2 [52.1-74.4]	30.6 [15.3-44.9]	1.9 [1.1-3.0]
<b>Experiment 2</b>				
Droplet size: 3 $\mu\text{L}$	1.7 [1.4-2.1]	62.9 [52.5-68.6]	19.5 [15.2-24.2]	0.5 [0.2-0.9]
Droplet size: 20 $\mu\text{L}$	3.3 [2.9-3.5]	63.1 [53.2-72.4]	41.2 [35.0-44.6]	0.6 [0.4-0.7]

### 5.3.3 Visualisation of results

The injection depth was compared between the direct and indirect injections and visualised by a boxplot in Figure 20. The cross within the boxplot indicates the mean value. The green boxplot shows the distribution of the direct injections, and the blue and purple boxplots specify respectively the indirect injections of 3  $\mu\text{L}$  and 20  $\mu\text{L}$ .

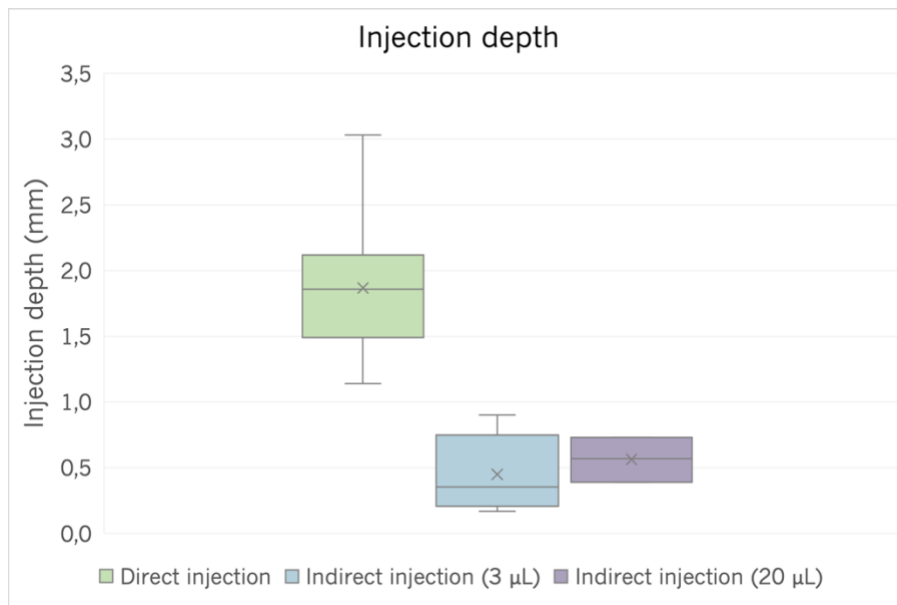


Figure 20: Comparison of the injection depth between the direct (green) and indirect injections (blue and purple). The grey cross indicates the mean value.

The scatter plots of injection depth and injection filling level as a function of microfluidic jet velocity for direct injections are respectively shown in Figures 21 and 22. The correlation between the injection depth and the microfluidic jet velocity was very low ( $R^2 = 0.15$ ). In addition, the correlation between the chamber filling level pre injection and the microfluidic jet velocity was also very low ( $R^2 = 0.19$ ). Scatter plots for indirect injections were not generated due to the small data set.

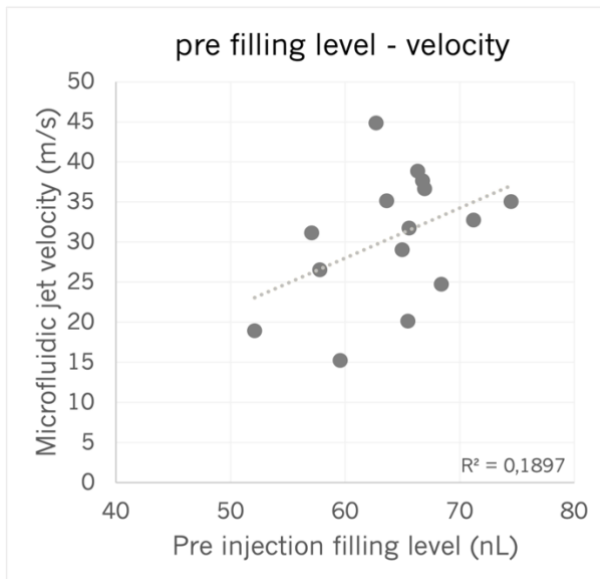


Figure 21: Scatter plot of the correlation between injection chamber filling level pre injection and the microfluidic jet velocity in direct injections.

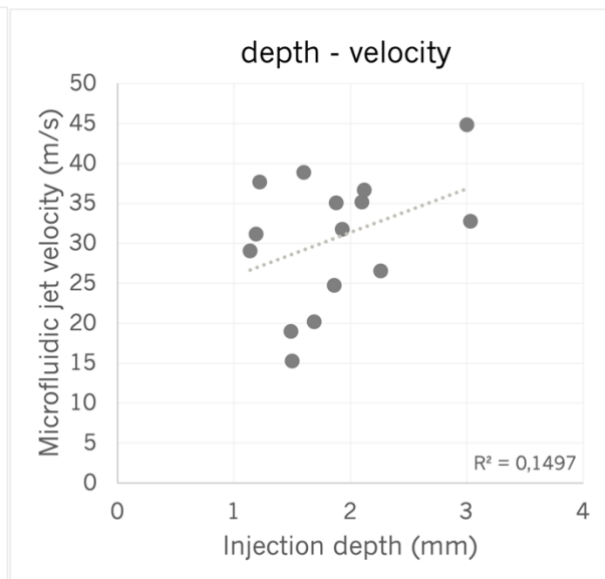


Figure 22: Scatter plot of the correlation between injection depth and the microfluidic jet velocity in direct injections.

## 5.4 Discussion

### 5.4.1 Results

Three important aspects will be discussed to explain the results and highlight potential differences between direct and indirect injections: timelapse, chamber filling levels and injection depth.

#### Timelapse

The timelapse showed dissimilarities in formation and behaviour of the jets between the direct and indirect injections. Two important characteristics must be highlighted: jet stability and splash-back. The microfluidic jet became unstable over time, broke up into smaller droplets and splashed back. This can be explained by the Plateau-Rayleigh instability: falling elongated liquid streams tend to minimize the surface tension by breaking up into smaller droplets which results in lower penetration power and splash-back.<sup>62,68</sup> The instability was observed in both the direct and indirect injections. The green droplet had a high surface tension which decreased the velocity of the microfluidic jet upon impact and caused splash-back. The surface tension of the agarose gel was lower and splash-back did not occur during the direct injections. It is unknown if the green dye is pulled along during indirect injection into the agarose gel, the red and green colour are not distinguishable on the high-speed camera images. Therefore, it cannot be concluded that the green dye is injected.

#### Chamber filling level

The chamber filling levels pre injection showed similar mean values for the direct and indirect injections. Literature describes that the filling level influences the velocity of the microjet. A lower injection filling level results in higher velocities because the bubble has to replace less liquid with the same amount of energy from the laser.<sup>69</sup> The scatter plot of the pre injection filling level and microjet velocity (Figure 21) shows a low correlation and a contradictory result: an increase in filling level resulted in an increase in velocity. This could be explained by the fact that the laser was not exactly aligned with the chamber resulting in energy loss. Another explanation could be the presence of small bubbles inside the chamber before injection. These bubbles absorbed a part of the energy from the laser and less energy can therefore contribute to the jet formation.

## Injection depth

Figure 22 shows the relation between microjet velocity and injection depth; higher depths were reached when the velocity increases although the correlation is low. This is in concordance with the findings of Krizek *et al.*<sup>67</sup> who described a linear relation between injection depth and jet speed. The mean and range values of the stand-off distance did not differ greatly between the direct and indirect injections; therefore the assumption was made that this variable did not influence potential differences in injection depth.

The boxplots visualise the differences in injection depth between direct and indirect injections. The data set was too small to perform statistical analysis but the boxplot and mean values show a higher depth applying direct injections (mean of 1.9 mm) compared to indirect injections (mean of 0.7 mm). This could be explained by the fact that the surface tension of the green droplet decreases the penetration efficacy resulting in lower depths.

### 5.4.2 Limitations

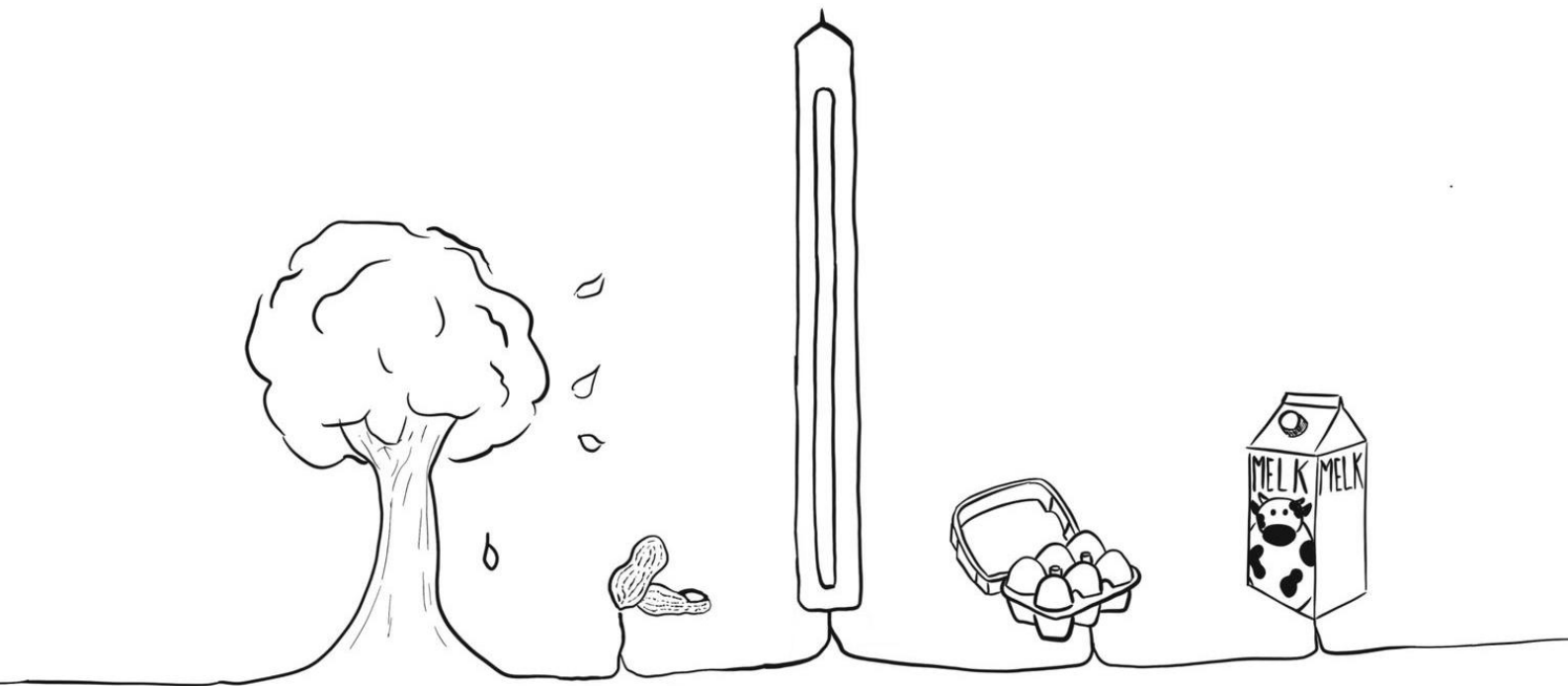
The first limitation is the size of the dataset; the final dataset includes 26 injections divided into three groups. Many injections were excluded because variables were unmeasurable as a result of complex illumination or software-related limitations. The recommendation is to expand the number of injections to validate the results. The second limitation is the quality of the high-speed camera images. The contrast and brightness were too low to distinguish the red and green dye and to measure the injection volume. Both variables could provide more information about the injection quality and the differences between direct and indirect injection and are therefore important to improve. Thirdly, the technology of the microjet injector could be improved regarding jet stability and speed to increase the injection efficacy and penetration depth. Moreover, the filling level must be investigated to find the optimal level that pushes all the volume out of the chamber during injection to prevent the formation of small bubbles. At last, the agarose gel could be replaced by a transparent skin phantom that mimics the characteristics of the epidermis.

## 5.5 Conclusion

This is the first pilot study that compared direct and indirect needle-free microjet injections to evaluate if the microjet injector is a convenient tool in the SPT. The results showed a lower injection depth applying indirect injections compared to direct injections. The green and red dye were not distinguishable and therefore it cannot be concluded if the green droplet is injected in the agarose gel during indirect injections. Future research is necessary and should focus on improving the microjet technology, enhancing the contrast and brightness of the high-speed camera images and investigating skin phantoms that mimic the characteristics of the epidermis.

# Chapter 6

## Impact and future recommendations



Returning to the research question posed at the beginning of this thesis, it is now possible to state that the injection depth is related to the wheal size in the SPT: an increase in injection depth leads to an increase in wheal size. This chapter discusses the clinical impact of these results, provides an overview of future recommendations into this topic and describes the conclusion of this research.

## 6.1 Clinical impact

In Deventer Hospital, the SPT is performed by multiple medical assistants and the lancet is manually pricked through the droplet into the epidermis. Two factors affect the SPT performance: 1) the injection depth is not limited by the horizontal shoulders of the lancet because the shoulders do not touch the skin during each injection, and 2) the medical assistants do not prick the lancet consistently into the skin which causes a variation in injection depth. A variation in injection depth causes a variation in wheal size. Currently, the wheal size is assessed as an indication of the level of sensitisation.<sup>9</sup> However, the wheal size does not only depend on the level of sensitisation, but also on the SPT performance. This could lead to an incorrect interpretation of a positive SPT in clinical practice. For example, when the histamine extract is pricked into the skin at a large depth and the food allergen extract at a small depth, the HEWS or mean diameter of the allergen extract wheal could be false negative. In this situation, the advice of the paediatrician could be to introduce the allergen at home while the child could develop an allergic reaction after ingestion. Conversely, when the histamine extract is pricked at a small depth and the allergen extract at a large depth, this could lead to overdiagnosis, medicalisation and unnecessary oral food challenges. These examples demonstrate the need to standardise the injection depth to obtain reproducible and reliable SPT results.

## 6.2 Future recommendations

The first step in standardising the SPT performance is to gain more knowledge about the skin structure. It is well known from previous studies that allergic children have an increased risk of developing atopic dermatitis which displays an impaired barrier function and an increased transepidermal water loss.<sup>70,71</sup> Compared to healthy skin, an atopic skin could be more permeable to histamine and allergen extracts which could result in larger wheals. In reviewing the literature, only one article described the association between atopic skin and the wheal size. Wagenpfeil *et al.* investigated in 1992 in a small cohort the size of histamine induced wheals between patients suffering from atopic eczema and allergic rhinitis.<sup>72</sup> The mean histamine wheal size was 35.93 mm<sup>2</sup> (standard deviation of 24.56 mm<sup>2</sup>) in the atopic eczema group and 20.78 mm<sup>2</sup> (standard deviation of 7.10 mm<sup>2</sup>) in the allergic rhinitis group which supports the hypothesis. In addition, the mast cell density in the forearm is important to investigate because this could affect the immunological reaction that is induced by the histamine or allergen extracts and could therefore influence the wheal size.

After the skin structure is explored, alternatives for the lancet could be considered. Until this day, no device can completely address all the controllable variables in the SPT. Current research is exploring possible alternatives for single- and multi-headed lancets and two techniques are worth highlighting: the Skin Prick Test Tape (SPT Tape) and microneedles. The SPT Tape is developed in 2019 by Gong *et al.* to overcome the limitations of the conventional SPT, such as cross-contamination and pain.<sup>73</sup> Moreover, SPT Tape is easy to apply, controls the penetration depth and has no appearance of needles. The design consists of an aluminium base with ten chambers, each with three microneedles, and a double-sided paste layer to close the chambers and tape the test on the forearm. The study tested the SPT Tape in subjects for house dust mites and the results were equivalent to the conventional SPT but no further research was published. Another alternative for the lancet is microneedles. Tran *et al.* designed and fabricated a biodegradable microneedle patch loaded with allergen extracts in 2020.<sup>74</sup> The technique was tested on porcine skin and the patch controlled the injection depth and was able to deliver a sufficient amount of extract into the skin. Further research is necessary to test the microneedle patch in subjects and explore clinical possibilities.

An example of a technology that could standardise the SPT performance, but is not investigated in this field yet, is an auto-injector.<sup>75</sup> The histamine or allergen extract is placed inside the liquid chamber and the pre-loaded coil compression spring pushes the extract through a needle into the epidermis. The design of the auto-injector must allow a fast change of needles and extracts or must be able to prick multiple allergens simultaneously into the skin. The spring is fixed at a certain length which provides a consistent needle length during injection. A number of studies investigated the factors that influence medication delivery by an auto-injector and they reported that not only the needle length but also Body Mass Index, obesity, tissue compression and propulsion affect the injection performance.<sup>76,77</sup> These studies used the auto-injector to administer medication intramuscular in the vastus lateralis muscle, so research is necessary to investigate what the effect of the beforementioned factors have on the allergen extract delivery during the SPT on the forearm. The principle of an auto-injector is illustrated in Figure 23.

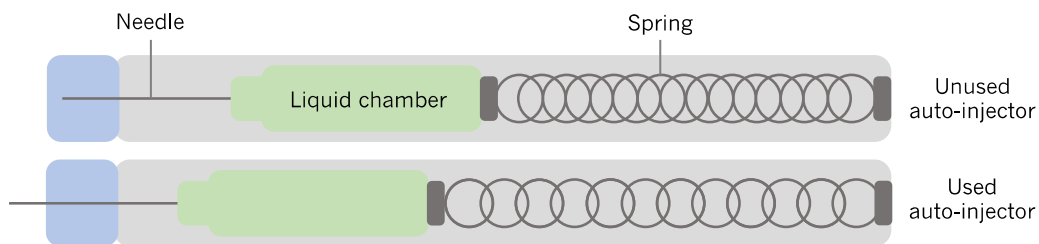


Figure 23: Illustration of an unused and used auto-injector.

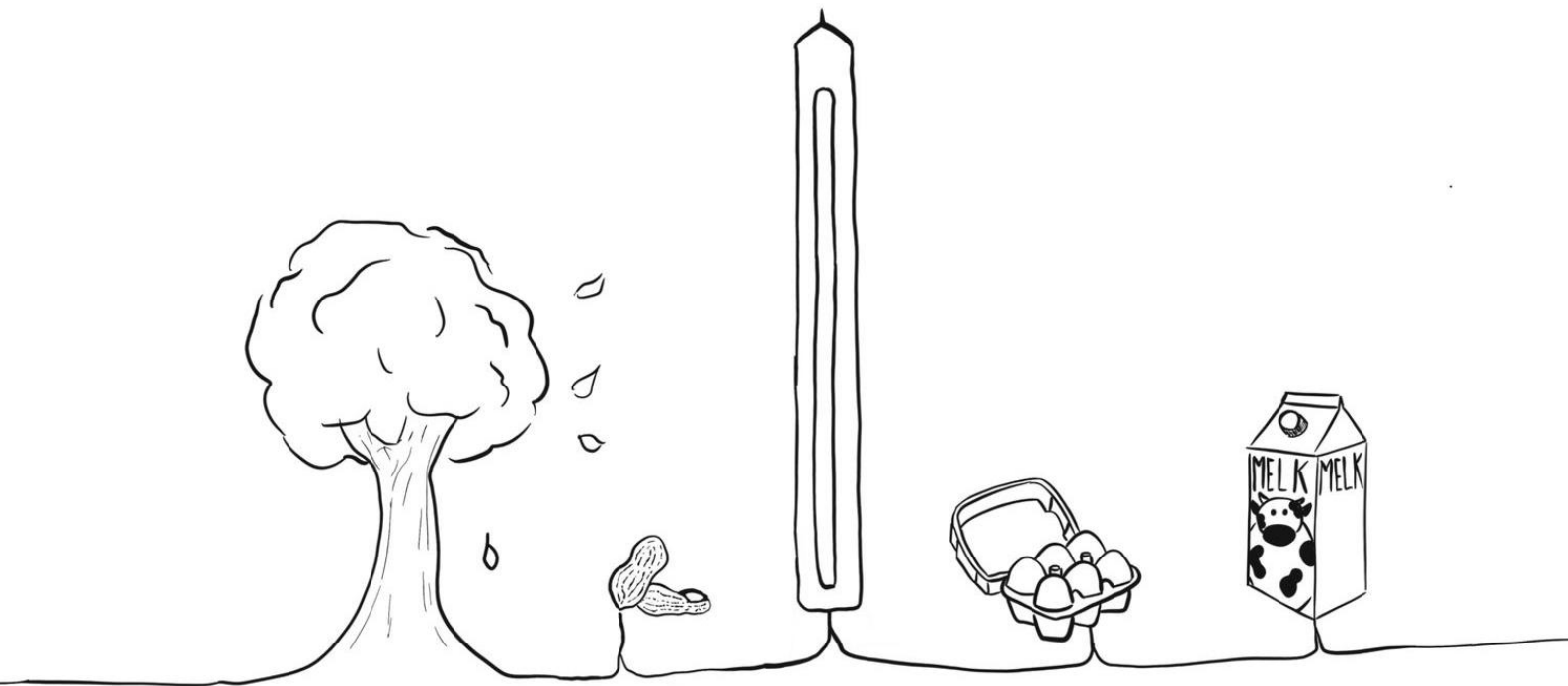
A device that could replace the lancet in the future is the needle-free injector, which is elaborated in Chapter 5. The technology needs further improvement before needle-free injections can be tested in humans but the needle-free injector shows possibilities to standardise the SPT performance in the future.

## 6.3 Conclusion

This thesis contributes to the knowledge regarding the effect of the injection depth and injection volume on the wheal size. This knowledge can be used to improve the reproducibility and reliability of the SPT. Experiments on *ex vivo* skin were executed to investigate the relation between the injection depth and injection volume. The influence of the injection depth on the wheal size was examined by performing SPTs on healthy volunteers. Taken together, the results show that an increase in injection depth leads to an increase in wheal size. This could result in an incorrect interpretation of the SPT results, overdiagnosis, medicalisation, unsafe home introduction of food products and unnecessary oral food challenges. Therefore, it is highly recommended to standardise the SPT performance. Future research could focus on investigating the skin structure and exploring devices to replace the lancet.

# Chapter 7

## References



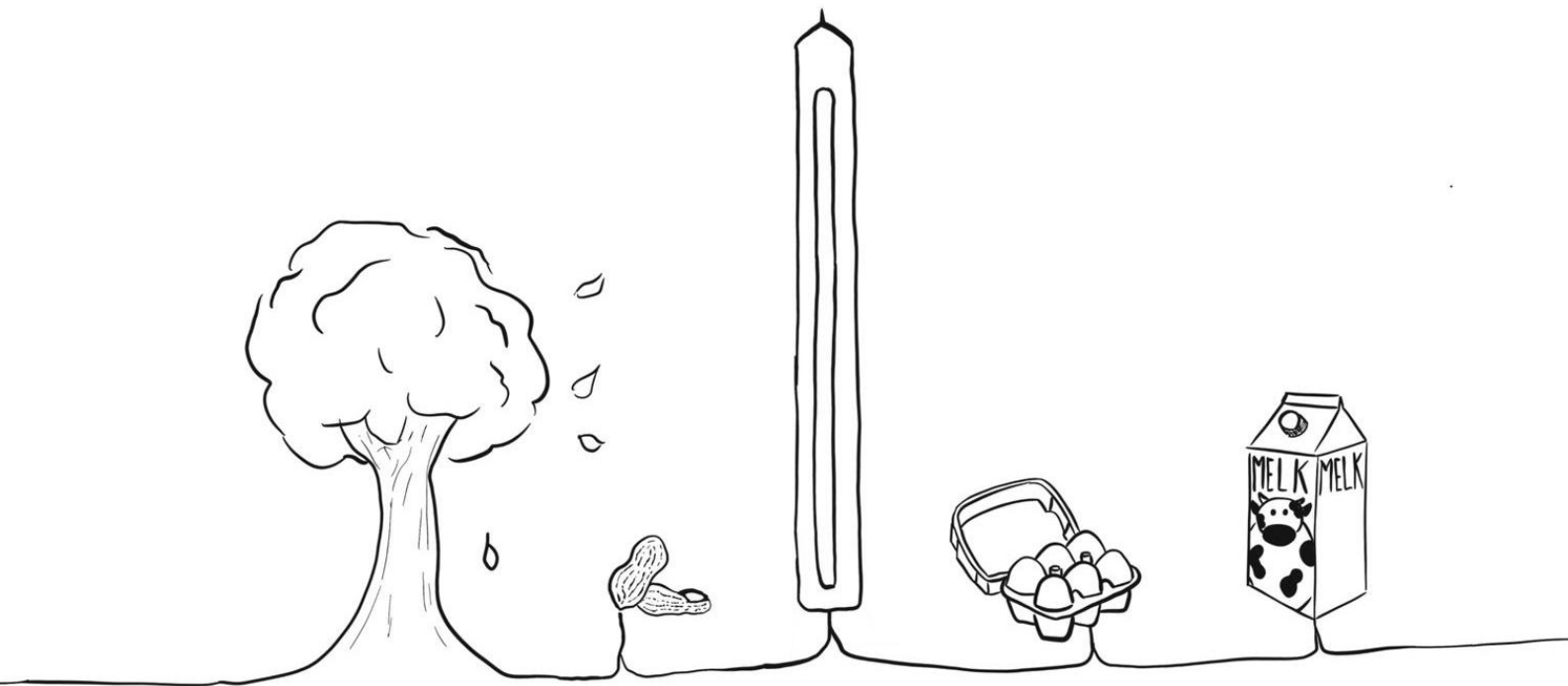
1. Sicherer, S. H. & Sampson, H. A. Food allergy: Epidemiology, pathogenesis, diagnosis, and treatment. *Journal of Allergy and Clinical Immunology* vol. 133 (2014).
2. Tang, M. L. K. & Mullins, R. J. Food allergy: is prevalence increasing? *Intern. Med. J.* 47, 256–261 (2017).
3. Abbas, M., Moussa, M. & Akel, H. Type I Hypersensitivity Reaction. *StatPearls* (2021).
4. Willett, C. Adverse Outcome Pathways: Development and Use in Toxicology. *Encycl. Toxicol. Third Ed.* 95–99 (2014) doi:10.1016/B978-0-12-386454-3.01244-6.
5. Delves, P. J. Hypersensitivity: IgE-Mediated (Type I). *eLS* 1–8 (2017) doi:10.1002/9780470015902.A0000965.PUB3.
6. Sheldon, J., Wheeler, R. D. & Riches, P. G. Chapter 30 – Immunology for clinical biochemists. in *Clinical Biochemistry: Metabolic and Clinical Aspects* (eds. Marshall, W. J., Day, A. P., Lapsley, M. & Ayling, R. M.) 560–603 (2014).
7. Heinzerling, L. *et al.* The skin prick test - European standards. *Clin. Transl. Allergy* 3, 1–10 (2013).
8. Greiner, A. N., Hellings, P. W., Rotiroti, G. & Scadding, G. K. Allergic rhinitis. *The Lancet* vol. 378 2112–2122 (2011).
9. Muthupalaniappen, L. & Jamil, A. Prick, patch or blood test? A simple guide to allergy testing. *Malaysian Fam. Physician* 16, 19–26 (2021).
10. Nederlandse Vereniging voor Klinische Chemie en Laboratoriumgeneeskunde. Allergie | NVKC. <https://www.nvkc.nl/zoek-eeen-test/?id=136> (2010).
11. Blackley, C. *Hay fever: its causes, treatment and effective prevention; experimental researches.* (1880).
12. Lewis, T. & Zotterman, Y. Vascular reactions of the skin to injury: Part VIII. The resistance of the human skin to constant currents, in relation to injury and vascular response. *J. Physiol.* 62, 280–288 (1927).
13. Mercuri, M. & Rivas, D. F. Challenges and opportunities for small volumes delivery into the skin. *Biomicrofluidics* vol. 15 011301 (2021).
14. Junqueira, L. C. Huid. in *Functionele Histologie* 493–495 (Reed Business Education, 2014).
15. Ito, Y. *et al.* Dissolving microneedles as skin allergy test device. *Biol. Pharm. Bull.* 40, 531–534 (2017).
16. Dioszeghy, V. *et al.* Antigen uptake by Langerhans cells is required for the induction of regulatory T cells and the acquisition of tolerance during epicutaneous immunotherapy in OVA-sensitized mice. *Front. Immunol.* 9, 1951 (2018).
17. Muraro, A., Werfel, T. & Hoffmann-Sommergruber, K. EAACI Food Allergy and Anaphylaxis Guidelines: Diagnosis and management of food allergy. *Allergy Eur. J. Allergy Clin. Immunol.* 69, 1008–1025 (2014).
18. de Jong, N. Huidtests. in *Werkboek Kinderallergologie* 49–53 (VU University Press, 2014).
19. Calvani, M., Bianchi, A., Reginelli, C., Peresso, M. & Testa, A. Oral food challenge. *Med.* 55, (2019).
20. Fatteh, S., Rekkerth, D. J. & Hadley, J. A. Skin prick/puncture testing in North America: A call for standards and consistency. *Allergy, Asthma Clin. Immunol.* 10, 44 (2014).
21. Doods, K. T., Keaney, D. L. & Dykewicz, M. S. Comparison of the Multi-Test II and ComforTen Allergy Skin Test Devices. *J. Allergy Clin. Immunol.* 123, S204–S204 (2009).
22. Buyuktiyaki, B. *et al.* Optimizing the use of a skin prick test device on children. *Int. Arch. Allergy Immunol.* 162, 65–70 (2013).
23. Kahveci, M. *et al.* Fine-tuning the use of a skin prick test device. *World Allergy Organ. J.* 13, (2020).
24. Tversky, J. R., Chelladurai, Y., McGready, J. & Hamilton, R. G. Performance and Pain Tolerability of Current Diagnostic Allergy Skin Prick Test Devices. *J. Allergy Clin. Immunol. Pract.* 3, 888–893 (2015).
25. Caimmi, D., Masse, M. S., Chiriach, A. M. & Demoly, P. Performances of an improved device for skin prick tests. *Int. J. Immunopathol. Pharmacol.* 26, 235–237 (2013).
26. Werther, R. L. *et al.* Variability in skin prick test results performed by multiple operators depends on the device used. *World Allergy Organ. J.* 5, 200–204 (2012).
27. Masse, M. S. *et al.* Comparison of five techniques of skin prick tests used routinely in Europe. *Allergy Eur. J. Allergy Clin. Immunol.* 66, 1415–1419 (2011).
28. Nelson, H. S., Lahr, J., Buchmeier, A. & McCormick, D. Evaluation of devices for skin prick testing. *J. Allergy Clin. Immunol.* 101, 153–156 (1998).
29. Nelson, H. S., Kolehmainen, C., Lahr, J., Murphy, J. & Buchmeier, A. A comparison of multiheaded devices for allergy skin testing. *Journal of Allergy and Clinical Immunology* vol. 113 1218–1219 (2004).
30. Carr, W. W., Martin, B., Howard, R. S., Cox, L. & Borish, L. Comparison of test devices for skin prick testing. *J. Allergy Clin. Immunol.* 116, 341–346 (2005).
31. Yoon, I. K., Martin, B. L. & Carr, W. W. A comparison of two single-headed and two multi-headed allergen skin test devices. *Allergy Asthma Proc.* 27, 473–478 (2006).
32. Andersen, H. H. *et al.* The lancet weight determines wheal diameter in response to skin prick testing with histamine. *PLoS One* 11, (2016).
33. Østerballe, O. & Weeke, B. A New Lancet for Skin Prick Testing. *Allergy* 34, 209–212 (1979).

34. Nahas, O., Mania Byron, G., Bourrain, J. L., Demoly, P. & Chiriac, A. M. Do we need more proofs for not using the same device for several subsequent skin prick tests? *Clinical and Experimental Allergy* vol. 49 1374–1378 (2019).
35. Carr, T. F. & Saltoun, C. A. Skin testing in allergy. in *Allergy and Asthma Proceedings* vol. 33 (Allergy Asthma Proc, 2012).
36. Valyasevi, M. A., Maddox, D. E. & Li, J. T. C. Systemic reactions to allergy skin tests. *Ann. Allergy, Asthma Immunol.* 83, 132–136 (1999).
37. Moneret-Vautrin, D. A. & Kanny, G. Anaphylaxis to muscle relaxants: Rational for skin tests. *Allerg. Immunol. (Paris)*. 34, 233–240 (2002).
38. Brockow, K. *et al.* General considerations for skin test procedures in the diagnosis of drug hypersensitivity. *Allergy Eur. J. Allergy Clin. Immunol.* 57, 45–51 (2002).
39. Niemeijer, N. R., Goedewaagen, B., Kauffman, H. F. & de Monchy, J. G. R. Optimization of skin testing: I. Choosing allergen concentrations and cutoff values by factorial design. *Allergy* 48, 491–497 (1993).
40. Al-Mujaini, A., Wali, U. K. & Azeem, S. Optical coherence tomography: Clinical applications in medical practice. *Oman Medical Journal* vol. 28 86–91 (2013).
41. Lodge, J. P. Fluorescence Spectrophotometry. in *Methods of Air Sampling and Analysis* 187–190 (2018). doi:10.1201/9780203747407-29.
42. Bajar, B. T., Wang, E. S., Zhang, S., Lin, M. Z. & Chu, J. A guide to fluorescent protein FRET pairs. *Sensors (Switzerland)* vol. 16 (2016).
43. Oppenheimer, J. & Nelson, H. S. Skin testing. in *Annals of Allergy, Asthma and Immunology* vol. 96 S6–S12 (Elsevier, 2006).
44. Dykewicz, M. S., Lemmon, J. K. & Keaney, D. L. Comparison of the Multi-Test II and Skintestor Omni allergy skin test devices. *Ann. Allergy, Asthma Immunol.* 98, 559–562 (2007).
45. Jeziorkowska, R., Rozalski, M., Skowroński, K. & Samochocki, Z. Can evaluation of specific immunoglobulin e serum concentrations of antibodies to aeroallergens in atopic dermatitis patients replace skin prick tests method in clinical practice? *Postep. Dermatologii i Alergol.* 36, 478–484 (2019).
46. Ravali, G. & Manivannan, M. Haptic Feedback in Needle Insertion Modeling and Simulation. *IEEE Reviews in Biomedical Engineering* vol. 10 63–77 (2017).
47. Gerovich, O., Marayong, P. & Okamura, A. M. The effect of visual and haptic feedback on computer-assisted needle insertion. *Comput. Aided Surg.* 9, 243–249 (2004).
48. Makvandi, P. *et al.* Engineering Microneedle Patches for Improved Penetration: Analysis, Skin Models and Factors Affecting Needle Insertion. *Nano-Micro Letters* vol. 13 1–41 (2021).
49. Pineda, J. *et al.* Robust automated reading of the skin prick test via 3D imaging and parametric surface fitting. *PLoS One* 14, (2019).
50. Van Der Valk, J. P. M. *et al.* Measurement and interpretation of skin prick test results. *Clin. Transl. Allergy* 6, 1–5 (2016).
51. Dreborg, S. Allergen skin prick test should be adjusted by the histamine reactivity. *Int. Arch. Allergy Immunol.* 166, 77–80 (2015).
52. Fujimoto, J. G. & Drexler, W. Introduction to Optical Coherence Tomography. in *Optical coherence tomography: Technology and applications* (Springer International Publishing, 2002). doi:10.1109/OMEMS.2002.1031485.
53. Jameson, D. M. *Introduction to Fluorescence*. (CRC Press, 2014).
54. Roseboom, I. C., Rosing, H., Beijnen, J. H. & Dorlo, T. P. C. Skin tissue sample collection, sample homogenization, and analyte extraction strategies for liquid chromatographic mass spectrometry quantification of pharmaceutical compounds. *Journal of Pharmaceutical and Biomedical Analysis* vol. 191 113590 (2020).
55. Dykewicz, M. S., Dooms, K. T. & Chassaing, D. L. Comparison of the Multi-Test II and ComforTen allergy skin test devices. *Allergy Asthma Proc.* 32, 198–202 (2011).
56. Blauw, A. *Protocol/werkwijze huidpriktesten (SPT)*.
57. Antunes, J., Borrego, L., Romeira, A. & Pinto, P. Skin prick tests and allergy diagnosis. *Allergologia et Immunopathologia* vol. 37 155–164 (2009).
58. Nelson, H. S., Knoetzer, J. & Bucher, B. Effect of distance between sites and region of the body on results of skin prick tests. *J. Allergy Clin. Immunol.* 97, 596–601 (1996).
59. Janssens, A. S. *et al.* Mast cell distribution in normal adult skin. *J. Clin. Pathol.* 58, 285–289 (2005).
60. Almeida, A. L. M. *et al.* Objective evaluation of immediate reading skin prick test applying image planimetric and reaction thermometry analyses. *J. Immunol. Methods* 487, 112870 (2020).
61. Chartier, Y. *et al.* *Safe management of wastes from health-care activities*. (2014).
62. Schoppink, J. & Fernandez Rivas, D. Jet injectors: Perspectives for small volume delivery with lasers. *Advanced*

- Drug Delivery Reviews* vol. 182 114109 (2022).
63. van der Ven, D. L., Morrone, D., Quetzeri-Santiago, M. A. & Rivas, D. F. Microfluidic jet impact: spreading, splashing, soft substrate deformation and injection. (2022).
  64. Berrospe-Rodríguez, C., Visser, C. W., Schlautmann, S., Ramos-García, R. & Rivas, D. F. Continuous-wave laser generated jets for needle free applications. *Biomicrofluidics* 10, 14104 (2016).
  65. Berrospe Rodríguez, C., Visser, C. W., Schlautmann, S., Rivas, D. F. & Ramos-García, R. Toward jet injection by continuous-wave laser cavitation. *J. Biomed. Opt.* 22, 1 (2017).
  66. Ham, H. C., Jang, H. J. & Yoh, J. J. A check valve controlled laser-induced microjet for uniform transdermal drug delivery. *AIP Adv.* 7, 125206 (2017).
  67. Krizek, J., Delrot, P. & Moser, C. Repetitive regime of highly focused liquid microjets for needle-free injection. *Sci. Rep.* 10, 1–9 (2020).
  68. de Gennes, P.-G., Brochard-Wyart, F. & Quéré, D. Capillarity: Deformable Interfaces. in *Capillarity and Wetting Phenomena* 1–31 (Springer, New York, NY, 2004). doi:10.1007/978-0-387-21656-0\_1.
  69. Oyarte Gálvez, L. *et al.* Microfluidics control the ballistic energy of thermocavitation liquid jets for needle-free injections. *J. Appl. Phys.* 127, 104901 (2020).
  70. Gold, M. S. & Kemp, A. S. Atopic disease in childhood. *Med. J. Aust.* 182, 298–304 (2005).
  71. Lee, H. J. & Lee, S. H. Epidermal permeability barrier defects and barrier repair therapy in atopic dermatitis. *Allergy, Asthma Immunol. Res.* 6, 276–287 (2014).
  72. Wagenpfeil, S., Grabbe, J., Jeep, S. & Czarnetzki, B. M. Reproducibility of skin prick test reactions to common allergens in patients with atopic eczema. *J. Allergy Clin. Immunol.* 89, 143–144 (1992).
  73. Gong, Z. *et al.* Comparison of a new Skin Prick Test Tape with the conventional skin prick test. *J. Allergy Clin. Immunol.* 143, 424–427 (2019).
  74. Tran, L. G. & Park, W. T. Rapid biodegradable microneedles with allergen reservoir for skin allergy test. *Micro and Nano Systems Letters* vol. 8 1–5 (2020).
  75. Access Spring. Coil Compression Springs for Auto-Injector Syringes. (2023).
  76. Song, T. T. & Lieberman, P. Epinephrine auto-injector needle length: What is the ideal length? *Current Opinion in Allergy and Clinical Immunology* vol. 16 361–365 (2016).
  77. Brown, J. C. Epinephrine, auto-injectors, and anaphylaxis: Challenges of dose, depth, and device. *Annals of Allergy, Asthma and Immunology* vol. 121 53–60 (2018).

# Chapter 8

## Appendix



# I. MATLAB script – injection depth

This script is used to determine the injection depth in MATLAB for the *ex vivo* experiments. The two files that need to be loaded are the XZ and YZ cross-sections of the pricking hole.

```
%% Injection depth

% Load file - adjust file name and scale
hard_XZ = imresize(imread('filename_XZ.tif'),[1000 2000]);
hard_YZ = imresize(imrotate(imread('filename_YZ.tif'),-90),[1000 2000]);

%% Hard_XZ
% Coordinates vertices - insert coordinates
Ax = 1039; Ay = 126; Bx = 1233; By = 94; Cx = 1149; Cy = 248;

% Injection depth: C to middle AB perpendicular
Dx = Ax + ((Bx-Ax)/2); Dy = By + ((Ay-By)/2);
Fy = Dy; Fx = Cx;
yellowLine = abs(Cy-Fy);

% Show images
figure, imshow(hard_XZ);
hold on
% Yellow Line
CF1 = [Cy,Cx]; CF2 = [Fy,Fx];
h(1) = plot([CF1(2),CF2(2)], [CF1(1),CF2(1)], 'Color','y','LineWidth',2, ...
    'DisplayName','Perpendicular Middle point');
% Point A, B and C
h(2) = plot(Ax, Ay, 'w.','MarkerSize', 15);
h(3) = plot(Bx, By, 'w.','MarkerSize', 15);
h(4) = plot(Cx, Cy, 'w.','MarkerSize', 15);
h(5) = plot(Dx, Dy, 'w.','MarkerSize', 15);
% Line AB
AB1 = [Ay,Ax]; AB2 = [By,Bx];
h(6) = plot([AB1(2),AB2(2)], [AB1(1),AB2(1)], 'Color','w','LineWidth',2);
% Line AC
AC1 = [Ay,Ax]; AC2 = [Cy,Cx];
h(7) = plot([AC1(2),AC2(2)], [AC1(1),AC2(1)], 'Color','w','LineWidth',2);
% Line BC
BC1 = [By,Bx]; BC2 = [Cy,Cx];
h(8) = plot([BC1(2),BC2(2)], [BC1(1),BC2(1)], 'Color','w','LineWidth',2);

%% Hard_YZ
% Coordinates vertices - insert coordinates
Ax = 1347; Ay = 74; Bx = 1597; By = 106; Cx = 1481; Cy = 246;

% Injection depth: C to middle AB perpendicular
Dx = Ax + ((Bx-Ax)/2); Dy = By + ((Ay-By)/2);
Fy = Dy; Fx = Cx;
yellowLine = abs(Cy-Fy);

% Show images
figure, imshow(hard_YZ);
hold on
% Yellow Line
CF1 = [Cy,Cx]; CF2 = [Fy,Fx];
h(1) = plot([CF1(2),CF2(2)], [CF1(1),CF2(1)], 'Color','y','LineWidth',2, ...
    'DisplayName','Perpendicular Middle point');
% Point A, B and C
h(2) = plot(Ax, Ay, 'w.','MarkerSize', 15);
h(3) = plot(Bx, By, 'w.','MarkerSize', 15);
h(4) = plot(Cx, Cy, 'w.','MarkerSize', 15);
h(5) = plot(Dx, Dy, 'w.','MarkerSize', 15);
% Line AB
AB1 = [Ay,Ax]; AB2 = [By,Bx];
h(6) = plot([AB1(2),AB2(2)], [AB1(1),AB2(1)], 'Color','w','LineWidth',2);
% Line AC
AC1 = [Ay,Ax]; AC2 = [Cy,Cx];
h(7) = plot([AC1(2),AC2(2)], [AC1(1),AC2(1)], 'Color','w','LineWidth',2);
% Line BC
BC1 = [By,Bx]; BC2 = [Cy,Cx];
h(8) = plot([BC1(2),BC2(2)], [BC1(1),BC2(1)], 'Color','w','LineWidth',2);
```

## II. Calibration curves

Figures 24 and 25 show the calibration curves of the porcine and human skin. These curves are used to convert the fluorescence signal of the skin samples to injection volumes.

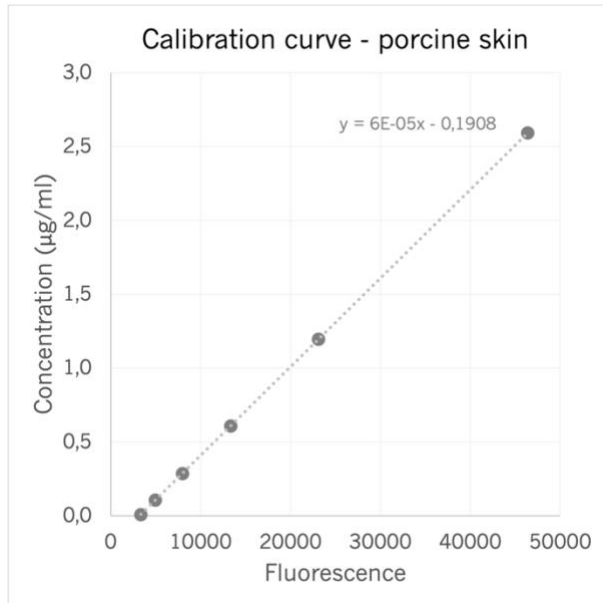


Figure 24: Calibration curve of the porcine skin experiments.

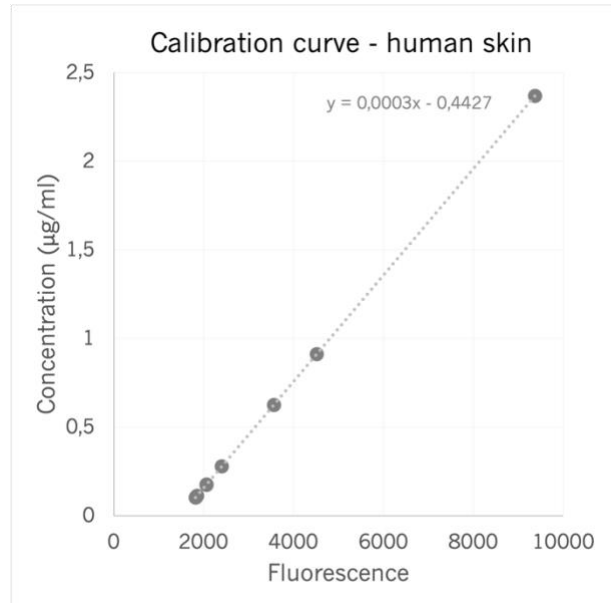


Figure 25: Calibration curve of the human skin experiments.

## III. MATLAB scrip – wheel size

### III.I Wheel surface

This script is used to determine the wheel size in MATLAB for the study in healthy volunteers. The first file that needs to be loaded is the overview image of the forearm to select the ArUco marker and the second file is the cropped segmented wheel.

```
%% Wheel surface
% Load file - adjust file name
aruco = imread(['filename.JPG']);
aruco = im2double(aruco);
figure, imshow(aruco);

% Select the four corner points of the aruco marker
point1 = drawpoint;
point2 = drawpoint;
point3 = drawpoint;
point4 = drawpoint;

cornerPoints = [point1.Position;
                point2.Position;
                point3.Position;
                point4.Position];

points = [cornerPoints(1,:); cornerPoints(2,:); cornerPoints(3,:)];

lengthPoints = sqrt(((points(2,1)-points(1,1))^2 + ((points(2,2)-points(1,2))^2));
widthPoints = sqrt(((points(3,1)-points(2,1))^2 + ((points(3,2)-points(2,2))^2));
lengthAruco = 12; % in mm
widthAruco = 12; % in mm

pixWidth = widthAruco/widthPoints; % in mm
pixHeight = lengthAruco/lengthPoints; % in mm
pixSurface = pixWidth*pixHeight; % in mm2

%% Pixel counting
% Load file - adjust file name
image = imread(['filename.png']);
image = im2double(image);
image = im2gray(image);
image = imbinarize(image, 0.99);

figure, imshow(image)
wheelsize = sum(image,'all') * pixSurface
```

## III.II Wheel diameter

This script is used to determine the mean wheel diameter in MATLAB for the study in healthy volunteers. The first file that needs to be loaded is the overview image of the forearm to select the ArUco marker and the second file is the cropped segmented wheel.

```
%% Pixel size
% Load file - adjust file name
aruco = imread(['filename.JPG']);
aruco = im2double(aruco);
figure, imshow(aruco);

% Select the four corner points of the aruco marker
point1 = drawpoint;
point2 = drawpoint;
point3 = drawpoint;
point4 = drawpoint;

cornerPoints = [point1.Position;
                point2.Position;
                point3.Position;
                point4.Position];

points = [cornerPoints(1,:); cornerPoints(2,:); cornerPoints(3,:)];
lengthPoints = sqrt(((points(2,1)-points(1,1))^2) + ((points(2,2)-points(1,2))^2));
widthPoints = sqrt(((points(3,1)-points(2,1))^2) + ((points(3,2)-points(2,2))^2));
lengthAruco = 12; % in mm
widthAruco = 12; % in mm

pixWidth = widthAruco/widthPoints; % in mm
pixHeight = lengthAruco/lengthPoints; % in mm
pixSurface = pixWidth*pixHeight; % in mm2

%% Wheel diameter
% Load file - adjust file name
image = imread(['PP020_L_S4_seg.png']); image = im2double(image); image = im2gray(image); image = imbinarize(image, 0.99);

% Find boundary pixels
[boundaries b] = bwboundaries(image);
boundaries = boundaries(1,1);
amountofboundarypixels = size(boundaries,1);
x = [];

% Calculate all distances between boundary pixels
for i = 1:amountofboundarypixels % start pixel
    pstart_x = boundaries(i,1);
    pstart_y = boundaries(i,2);
    for ii = 1:amountofboundarypixels % measurement pixels
        ppoint_x = boundaries(ii,1);
        ppoint_y = boundaries(ii,2);
        distancebetweentwopoints(ii) = sqrt(((pstart_x - ppoint_x)^2) + ((pstart_y - ppoint_y)^2));
        x = [x, distancebetweentwopoints(ii)];
        [diameter1 index_max1] = max(x);
    end
end

x = reshape(x,[amountofboundarypixels,amountofboundarypixels]);
[index_ppoint, index_pstart] = ind2sub(size(x),index_max1);

% Find the two coordinates of the maximum diameter
coordinates_ppoint = boundaries(index_ppoint,:);
coordinates_ppoint_x = coordinates_ppoint(1,2);
coordinates_ppoint_y = coordinates_ppoint(1,1);

coordinates_pstart = boundaries(index_pstart,:);
coordinates_pstart_x = coordinates_pstart(1,2);
coordinates_pstart_y = coordinates_pstart(1,1);

% Rotate image to align with the maximum diameter
angle = asind((abs(coordinates_pstart_x - coordinates_ppoint_x))/diameter1);
image_rotate = imrotate(image,angle);
summation = sum(image_rotate,2);
[diameter2 index_max2] = max(summation);

% Calculate mean histamine wheel diameter
diameter1 = diameter1 * ((pixHeight+pixWidth)/2) % in mm
diameter2 = diameter2 * ((pixHeight+pixWidth)/2) % in mm
diameterwheel = ((diameter1 + diameter2)/2) % in mm
```

## IV. Overview of the segmentation steps

Figure 26 shows an overview of the segmentation steps. First, the images of the forearms were edited to increase the contrast and adjust the visibility of the wheals. The images were then cropped to individual wheals and each wheal was manually segmented. The segmentations were converted to binary images and pixel counting was applied to determine the wheal size.

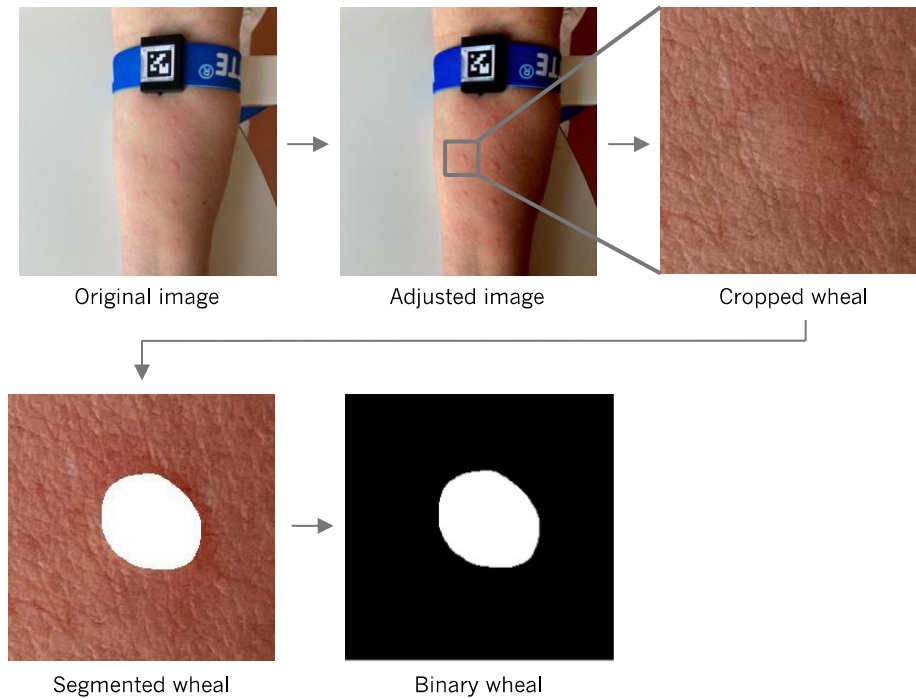


Figure 26: Overview of the segmentation steps.